Anti-Remodeling and Anti-Fibrotic Effects of the Neuregulin-1β Glial Growth Factor 2 in a Large Animal Model of Heart Failure

Cristi L. Galindo, PhD;* Ehab Kasasbeh, MD;* Abigail Murphy, BA; Sergey Ryzhov, MD, PhD; Sean Lenihan; Farhaan A. Ahmad, MD; Philip Williams, PhD; Amy Nunnally, BS; Jamie Adcock, BS; Yanna Song, PhD; Frank E. Harrell, PhD; Truc-Linh Tran, BS; Tom J. Parry, PhD; Jen Iaci, MS; Anindita Ganguly, PhD; Igor Feoktistov, MD, PhD; Matthew K. Stephenson, PhD; Anthony O. Caggiano, MD, PhD; Douglas B. Sawyer, MD, PhD;[†] John H. Cleator, MD, PhD[†]

Background—Neuregulin-1β (NRG-1β) is a growth factor critical for cardiac development and repair with therapeutic potential for heart failure. We previously showed that the glial growth factor 2 (GGF2) isoform of NRG-1β improves cardiac function in rodents after myocardial infarction (MI), but its efficacy in a large animal model of cardiac injury has not been examined. We therefore sought to examine the effects of GGF2 on ventricular remodeling, cardiac function, and global transcription in post-MI swine, as well as potential mechanisms for anti-remodeling effects.

Methods and Results—MI was induced in anesthetized swine (n=23) by intracoronary balloon occlusion. At 1 week post-MI, survivors (n=13) received GGF2 treatment (intravenous, biweekly for 4 weeks; n=8) or were untreated (n=5). At 5 weeks post-MI, fractional shortening was higher (32.8% versus 25.3%, *P*=0.019), and left ventricular (LV) end-diastolic dimension lower (4.5 versus 5.3 cm, *P*=0.003) in GGF2-treated animals. Treatment altered expression of 528 genes, as measured by microarrays, including collagens, basal lamina components, and matricellular proteins. GGF2-treated pigs exhibited improvements in LV cardiomyocyte mitochondria and intercalated disk structures and showed less fibrosis, altered matrix structure, and fewer myofibroblasts (myoFbs), based on trichrome staining, electron microscopy, and immunostaining. In vitro experiments with isolated murine and rat cardiac fibroblasts demonstrate that NRG-1β reduces myoFbs, and suppresses TGFβ-induced phospho-SMAD3 as well as αSMA expression.

Conclusions—These results suggest that GGF2/NRG-1β prevents adverse remodeling after injury in part via anti-fibrotic effects in the heart. (*J Am Heart Assoc*. 2014;3:e000773 doi: 10.1161/JAHA.113.000773)

Key Words: extracellular matrix • fibroblasts • fibrosis • myocardial infarction • neuregulin

Neuregulin-1β (NRG-1β) is a growth and survival factor that belongs to the family of epidermal growth factors (EGF) critical for cardiac development.[1] In the adult heart,

From the Division of Cardiovascular Medicine, Department of Medicine, Vanderbilt University Medical Center, Nashville, TN (C.L.G., E.K., A.M., S.R., S.L., F.A.A., P.W., A.N., J.A., T.-L.T., I.F., D.B.S.); Departments of Pharmacology (J.H.C.) and Biostatistics (Y.S., F.E.H.), and Ingram Cancer Center (M.K.S.), Vanderbilt University, Nashville, TN; Acorda Therapeutics, Ardsley, NY (T.J.P., J.I., A.G., A.O.C.).

*Dr Galindo and Dr Kasasbeh contributed equally to the manuscript.

[†]Dr Sawyer and Dr Cleator contributed equally to the manuscript.

An accompanying Table S1 is available at http://jaha.ahajournals.org/content/3/5/ e000773/suppl/DC1

Correspondence to: Douglas B. Sawyer, MD, PhD, Division of Cardiovascular Medicine, Department of Medicine, Vanderbilt University Medical Center, 2220 Pierce Avenue, Room #383, Preston Research Building, Nashville, TN 37232. E-mail: douglas.b.sawyer@vanderbilt.edu

Received May 5, 2014; accepted September 15, 2014.

NRG-1β is a stress-activated mediator of cardiac repair after injury. Recombinant NRG-1β is being investigated as a potential therapeutic for heart failure. In rats with myocardial injury induced by coronary artery ligation, IV doses of the EGF-like domain of NRG-1β given daily for 4 weeks post-infarction improved cardiac function.[2] In humans with stable chronic heart failure, administration of this same NRG-1β improves hemodynamics acutely and systolic function both acutely and chronically.[3,4]

A full-length recombinant NRG-1β3 Glial Growth Factor 2 (GGF2) is also being examined as a possible treatment for cardiovascular disease. Similar to the EGF-like domain of NRG-1β, dose-ranging safety studies of GGF2 have been conducted in ex vivo cell culture models and small animals, but not large animals. GGF2 improves survival of isolated adult rat ventricular cardiomyocytes,[5] and improves cardiac function in post-MI rodents.[6] The effect of NRG-1β on diastolic function and inotropic reserve in heart failure has not been examined. Consequently, we conducted a study in swine with post-myocardial infarction remodeling, where the primary endpoint was evaluation of cardiac structure and

function as assessed by quantitative echocardiography and invasive, intraventricular hemodynamic measurements.

In addition to increasing systolic function, we found that GGF2 also prevented remodeling. To investigate the underlying mechanisms for this effect, we performed microarray analysis on non-infarcted left ventricular myocardium from GGF2-treated and untreated swine. Among the many changes, a striking effect was found on matricellular genes involved in fibrosis. We explored this effect further in both the swine tissue and isolated cardiac fibroblasts to better characterize the mechanisms for the anti-remodeling and anti-fibrotic role of this signaling system.

Methods

Animals

This study was approved by the Vanderbilt Institutional Animal Care and Use Committee (IACUC, protocols number M/10/117 [swine] and M/10/219 [rat and mice]) and conducted according to Association for the Accreditation of Laboratory Animal Care (AAALAC) International standards. Male, castrated Yorkshire swine (mean weight of 54.5 kg, age <1 year) were acclimated and received 400 mg of oral amiodarone once daily 7 to 14 days prior to infarction. Myocardial infarction was induced by angiographically guided intracoronary balloon occlusion for 60 minutes (see below). From 7 to 35 days post-MI, swine were treated with 8 doses of intravenous NRG-1β (GGF2 isoform, Acorda Therapeutics, Inc, in vehicle stock solution: 20 mmol/L histidine, 100 mmol/L arginine, 100 mmol/L sodium sulfate, 1% mannitol, pH 6.5) every 3 to 4 days. Swine surviving until completion of the protocol were euthanized by barbiturate overdose (pentobarbital, 125 mg/kg) after completion of the final analyses of cardiac function.

Thirteen of 23 swine completed the study, 5 untreated and 8 treated. MI was confirmed by electrocardiography in all animals during balloon occlusion of the left anterior descending artery. Twelve of the swine developed ventricular fibrillation during induction of MI. In 8 swine this was refractory to cardioversion and resuscitative efforts, giving an acute mortality of 38%, similar to other studies in swine.[7] Serum troponin I levels were undetectable prior to the procedure, and increased to 38.3 ± 16 μg/L at 5 to 16 hours after completion of the myocardial infarct. One animal died 3 days after induction of the MI, and necropsy indicated peritonitis as the probable cause of death. One animal in the treatment group developed erratic movements that were clinically interpreted by veterinary staff as due to a stroke at 17 days post-MI and was euthanized. Anterior-apical wall motion abnormality was evident in all surviving swine in the baseline echocardiograms performed 7 days post-MI.

Induction of myocardial infarction

Anesthesia was induced by intramuscular injection of ketamine/xylazine (2.2 mg/kg), telazoll (4.4 mg/kg), and atropine (0.05 mg/kg) then maintained by inhaled 1% to 3% isoflurane after intubation. The right femoral artery was exposed surgically, and a 6F arterial sheath was inserted using a modified version of the Seldinger technique. After infusion of heparin (200 U/kg), swine received an intravenous amiodarone bolus (300 mg). Lidocaine (0.5 mg/min) and amiodarone (1 mg/min) IV were infused throughout the procedure to prevent ventricular arrhythmias. The amiodarone infusion rate was halved if the heart rate dropped below 60 beats per minute. Maintenance heparin boluses (20 U/kg) were administered every hour. A 6F Hockey Stick guide (Mach 1 peripheral Guide Catheter, 0.070″ internal diameter, shaft length 55 cm, Boston Scientific) was used to engage the left main coronary artery. Angiography was performed by intracoronary injection of contrast media (Omnipaque or Visipaque). A 0.014″ coronary guidewire was fluoroscopically guided to the left anterior descending coronary artery (LAD), and a 3.5×15 mm balloon was inflated at occlusive pressure (4 to 6 atm) just distal to the first diagonal branch. Repeat angiography was performed to ensure complete occlusion of the LAD, and the balloon remained in occlusive position for 60 minutes. If ventricular fibrillation occurred during the infarct, then direct current cardioversion (200 J) was delivered using external paddles. Electrocardiograms were acquired pre-procedure and during the infarction at 1, 5, 30, and 60 minutes to confirm myocardial injury. To account for clockwise rotation of the swine heart,[8] V1 and V2 were placed to the right of the sternum, while the remaining leads were positioned in the standard 12-lead fashion. Serum troponin I levels (Abbott I Care troponin cartridge) were measured before and 5 to 16 hours after induction of MI. Swine were assessed twice daily during the first week after MI. Ketaprofen (3.0 mg/kg) was administered intramuscularly for 2 days for post-operative analgesia.

NRG-1β treatment

Access to the jugular vein for delivery of intravenous NRG-1β was achieved by implanting chronic indwelling ear vein catheters under general anesthesia after acquiring echocardiographic images at 7 days post-MI. The cannulae were placed under aseptic conditions in either the lateral or medial auricular vein, depending on vessel prominence and accessibility. A long-term MILA International catheter (radiopaque polyurethane, 19 G, 25 cm) was inserted. Correct insertion was affirmed by aspiration of blood with a syringe. Catheters were subsequently flushed with sterile glycerin, heparin solution (1:1) and fixed into place with sutures. Animals were assigned to treated and untreated groups upon survival at 1 week post-MI.

The glial growth factor 2 isoform of NRG-1β (GGF2) was provided by Acorda Therapeutics, Inc (96.0% purity by SEC-HPLC), in vehicle stock solution (20 mmol/L histidine, 100 mmol/L arginine, 100 mmol/L sodium sulfate, 1% mannitol, pH 6.5), stored at 4°C until use. From 7 to 35 days post-MI, swine were treated with 8 doses of intravenous GGF2 (twice a week, every 3 to 4 days). The first dose (initial intended dose of 2 mg/kg reduced to 0.67 mg/kg, see below) was administered under anesthesia after echocardiography and catheter insertion procedures were completed. The remaining 7 doses were administered in conscious animals. GGF2 was infused into the central venous catheters by way of IV extension sets (Smiths Medical, 60″, APV=1.8 mL) over 15 minutes.

The catheter lines were flushed with normal saline, followed by 1 mL of glycerin/heparin solution. Catheters were used to collect blood samples for electrolyte analysis by an outside lab (Antech Diagnostics). An acute transient hypoglycemic response to GGF2 was observed as described in Results, leading to protocol modifications in consultation with veterinary staff. These modifications included use of intravenous 50% dextrose solution (0.5 g/mL) to treat hypoglycemia, and overnight fasting to reduce risk of emesis. After 2 swine completed the protocol in the treatment group, there was a dose reduction from 2 to 0.67 mg/kg, which was better tolerated. Overnight fasting was discontinued with the low-dose swine as emesis was not a reaction symptom.

For cell culture studies, recombinant NRG-1β (R&D) was used at a dose of 50 μg/mL, unless otherwise specified. When administered in vitro, NRG-1β treatment was carried out in the absence of serum.

NRG-1β/GGF2 treatment tolerability

An initial dose of GGF2 of 2.0 mg/kg, twice per week, was selected as the maximum feasible dose based upon stock GGF2 concentration, and a dose consistent with effective doses in rodent studies.[6] The first 2 swine in the treatment group were noted to develop transient lethargy with vomiting, occurring within 15 minutes of treatment, persisting 60 to 90 minutes after treatment, with complete resolution of symptoms and normal behavior between doses. Blood samples drawn early after GGF2 hypoglycemia (20 mg/dL, normal range of 48 to 145 mg/dL), without electrolyte abnormalities. Prophylactic measures developed in consultation with veterinary staff (details in Methods) reduced the severity of the lethargy and prevented vomiting and convulsions. After the first 2 swine completed the full course of the study with 8 doses of 2 mg/kg GGF2 a decision was made to lower the dose of GGF2 to 0.67 mg/kg, which was better tolerated. As this dose reduction was used to improve animal

tolerability and not to determine dose-response characteristics, data from all treated swine were analyzed as a group, and compared with untreated swine.

Assessment of Cardiac Function

Echocardiographic images were obtained at 7 and 35 days post-MI in swine under general anesthesia as described above. The left ventricular inner dimension at end-diastole and end-systole (in centimeters) were measured in the parasternal long-axis view and used to calculate the left ventricular fractional shortening. Measurements of the left ventricular septal wall and posterior wall were taken in the same view. In cases where image quality of the parasternal long-axis was compromised, a short-axis slice through the mid-left ventricular cavity was used to measure the left ventricular end-diastolic and systolic dimensions for calculation of fractional shortening. Analysis of all 2-D echocardiogram images in DICOM formatted datasets was performed using the OsiriX (open-source) program. Echocardiograms were interpreted by a cardiologist with advanced echocardiography training (F.A.) who was kept blinded to the treatment group.

Assessment of cardiac function by intraventricular hemodynamics

At 35 days post-MI, swine were placed under general anesthesia as described above, and after re-evaluating cardiac function by echocardiography, the right common carotid artery was accessed for delivery of 5 French 7-electrode conductance catheter (MPVS Ultra system; Millar Instruments Inc) to the left ventricle under fluoroscopic guidance. Digital signals were stored in computer memory through an analog-digital interface (AD Instruments Inc; Colorado Springs, CO) at a sampling rate of 500 Hz. Hemodynamic assessment of LV contractility was achieved by pressure volume analysis and measurements of the first derivative or rate of change of ventricular pressure (dP/dt maximum and minimum in units of mm Hg/ms). Hemodynamic assessment of LV function also included the following parameters: left ventricular ejection fraction (LVEF%), left ventricular end systolic volume (LVESV), left ventricular end diastolic volume (LVEDV), stroke volume (SV), left ventricular end diastolic pressure (LVEDP), and heart rate. These measurements were acquired in all study animals (untreated or repeat-dose GGF2-treated) under rest conditions and in response to dobutamine challenge both before and 20 minutes after acute GGF2 challenge. Dobutamine challenge was completed by continuously infusing incremental doses of dobutamine (5, 10, 20, & 40 μg/kg per minute) for 3 minutes each in a stepwise fashion.

Microarrays

Assessment of left ventricular RNA (collected remote from the site of infarct), hybridization to Affymetrix porcine genome arrays, and data acquisition was performed by the GSR Microarray Core at Vanderbilt. One animal per array (3 untreated and 5 GGF2-treated animals) was used, and data were analyzed as previously described using Partek Genomics Suite 6.6.[6] Remote LV tissue was homogenized and total RNA subsequently extracted using a Qiagen RNeasy kit. Quality Assessment of RNA, further processing, and data acquisition was performed by the GSR Microarray Core at Vanderbilt. Raw data were RMA normalized, followed by ANOVA with Benjamini & Hochberg correction, using Partek Genomics Suite 6.6. Genes with a *P* value (with or without FDR) <0.05 and fold-diff >1.5 were considered significantly altered.

To characterize differential transcripts for which swine gene information was unavailable, probe source sequences obtained from the Affymetrix NetAffx website (www.affymetrix.com) were manually searched against the human reference genome using the UCSC Genome Bioinformatics' tool, BLAT. BLAT differs from BLAST in that it uses an index consisting of all non-overlapping, non-repetitive 11-mers and is derived from assembly of the entire genome. To minimize false positives, only alignments >70% yielding a score >100 were considered as potentially orthologous. The results of this analysis are included.

For comparison to human heart failure, repository data was obtained from the ArrayExpress Archive, which is hosted by European Molecular Biology Laboratory of the European Bioinformatics Institute (http://www.ebi.ac.uk/arrayexpress/) and Gene Expression Omnibus, available through the NCBI (http://www.ncbi.nlm.nih.gov/geo/). Each data set was separately normalized and compared with experimentally matched controls. The resulting lists were then combined for comparison with swine gene expression data. Comparison with microarray results from our previous rat experiments examining the effects of NRG-1β–treatment post-MI was similarly accomplished.

Real-Time RT-PCR

Custom primers (Table 1) were designed using Primer3 (http://frodo.wi.mit.edu) and purchased from Invitrogen. Relative gene expression was assessed using the QuantiTect One-Step SYBR Green RT-PCR kit (Qiagen) for selected genes in a Bio-Rad CFX instrument, according to manufacturer's protocol. Briefly, ≈100 ng of RNA was mixed with RT master mix, RT enzyme, RNase-free water, and 0.5 μmol/L each of forward and reverse primer, for a total reaction volume of 10 μL. A typical protocol included reverse transcription for 30 minutes at 50°C, PCR activation for 15 minutes at 95°C, and 50 cycles as follows: denaturation (15 seconds at 95°C), annealing (30 seconds at 60°C), and extension with data acquisition (30 seconds at 72°C). The comparative threshold method[9] was used to calculate fold-differences. Two custom GAPDH primers served as internal controls to normalize target gene expression across different samples. We compared samples from 3 untreated swine, as well as 5 samples from treated swine that included the first 2 swine receiving higher dose GGF2, and 3 swine treated with the subsequent dose.

Table 1. Primers for Real-Time RT-PCR

Gene	Forward Primer Sequence (5′→3′)	Reverse Primer Sequence (5′→3′)
Col1a2	CCTCGGCAACAGTCACTCA	GGATGAAGAGATGGCAACTGAA
Col3a1	GCCTCAAGGCTTTCTTTACATTCC	GCTTCCCAGAACATCACATATCAC
Col4a1	GCTCTCCTGCTGAAGTCTGAAC	GCGGGAGAAACAGCTCTGTC
Col5a2	CTTCACGATACTTGCTCTAAACGA	AGCGTGCCACATTCTGTGTTC
Col12a1	GCCCTCTCAACATACACAGTAGT	GGGCAGCCTCAGTGAAAC
Gadd45B	CGACTGGATGAGGGTGAAGTG	AGTCGGCCAAGCTGATGAATG
MyoCd	CCGGCCACTTGGGAACAC	CACTGCGGGCTGAGAAACG
FosB	GGACGGGTCAGTGGAATGTTT	CTGTGCTTCACCTCGGAGAATT
Nr2a4	ACAAGCCTTTGCCTTCTTCAAC	GGACCCACAAGTATTGCCCTTTA
Areg	GCACCTGGAAGCAGTAACCTG	TGGTGTGAGTCTTCATGGACTT
KLF5	GAACGTCTTCCTCCCTGACATC	CGCACGGTCTCTGGGATT
GAPDH	CACTGCACAGCCCTTAACTC	CTGCTGCGGCAACCTTTAAC
GAPDH	TGGGCGTGAACCATGAGAAG	GGTGGTGCAGGAGGCATT

RT-PCR indicates reverse transcriptase polymerase chain reaction.

At least 3 technical replicates for each sample were also included to ensure reproducibility.

Immunohistochemistry

LV tissue pieces (collected remotely from the site of infarct) were embedded in OCT, sectioned into 5 μmol/L thick slices, placed on slides, and stored at −20°C. Before staining, slides were allowed to air dry at room temperature for 45 min, followed by fixation in 4% paraformaldehyde for 45 minutes at room temperature. Slides were washed 4 times for 15 minutes each in PBS, permeabilized in 0.5% triton X-100 in PBS for 1 hour, washed, and then blocked in 1% BSA in PBS for 1 hour. Slides were again washed (4 times, 15 minutes each) prior to overnight incubation in primary antibody at 4°C in the

dark. Primary antibodies included rabbit anti-collagen IV (Abcam), diluted 1:100 in 1% BSA in PBS, anti-rabbit collagen I (Rockland) diluted 1:4500 in 1% BSA, or FITC-conjugated anti-actin, α smooth muscle (αSMA), clone 1A4 (Sigma-Aldrich) diluted 1:1000 in 1% BSA in PBS. After washing, collagen IV-stained slides were incubated for 1 hour at room temperature in 1% BSA in PBS with 1:1000 Alexa Fluor® 488 Goat Anti-Rabbit IgG (H+L) (Invitrogen Life Technologies) and 1:1000 Texas Red®-X Phalloidin (Invitrogen Life Technologies). Slides stained with FITC-αSMA were incubated with phalloidin only (1:1000 in 1% BSA in PBS for 1 hour). After 4 final washes, slides were mounted using ProLong® Gold Antifade Reagent with DAPI (Invitrogen Life Technologies), covered, and visualized using an Olympus IX81 fluorescence microscope.
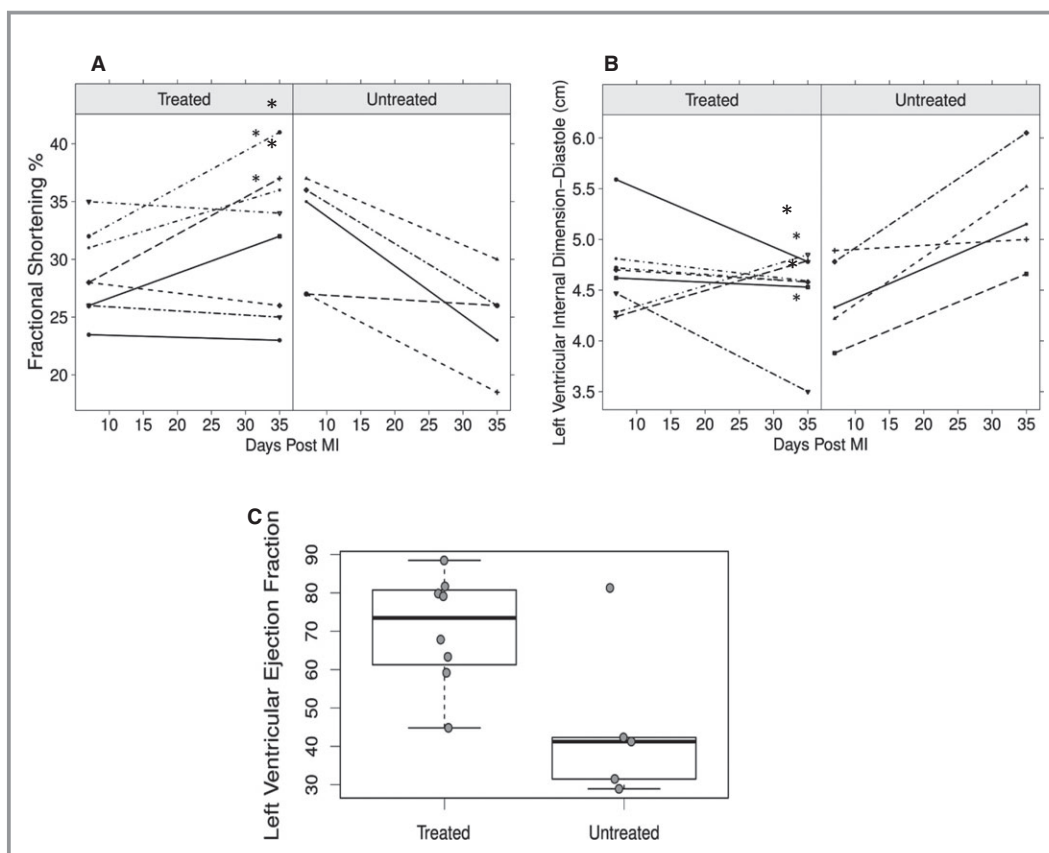

Figure 1. Representative effect of GGF2 treatment on left ventricular function by echocardiography. Individual subject fractional shortening % (A) and LVIDd (B) change over time is shown stratified by treatment group. There was no difference in LV dimensions (FS% *P*=0.172, LVIDd *P*=0.309) between groups before GGF2 treatment, at 7 days post-infarct. At 35 days post-MI, FS% and LVIDd were significantly different in GGF2-treated animals (FS% *P*=0.019, LVIDd *P*=0.003). C, GGF2 was associated with improved ejection fraction, as estimated by Millar Pressure-Volume recordings, compared the untreated animals (*P*=0.033). *Denotes animals receiving the higher dose of GGF2 before dose reduction. FS indicates fractional shortening; GGF2, glial growth factor 2; LVIDd, left ventricular inner diameter at diastole; MI, myocardial infarction.

Table 2. Echocardiographic Measurements

	Treated (N=8)			Untreated (N=5)			Treated vs Untreated Test Stat	
	Day 7	Day 35	Test Stat	Day 7	Day 35	Test Stat	Day 7	Day 35
LVIDd, cm	4.42 [4.68] 4.74	4.57 [4.53] 4.78	P=0.41	4.22 [4.42] 4.78	5.00 [5.28] 5.52	P=0.0003	P=0.31	P=0.003
LVIDs, cm	3.16 [3.34] 3.39	2.86 [3.08] 3.25	P=0.14	2.83 [3.00] 3.06	3.87 [3.98] 4.08	P=0.90	P=0.13	P=0.43
FS	24.5 [29.1] 32.6	29.4 [32.9] 35.7	P=0.04	28.6 [33.0] 36.5	15.2 [25.3] 30.6	P=0.002	P=0.17	P=0.019
IVS, cm	0.71 [0.81] 0.88	0.81 [0.95] 1.1	P=0.04	0.81 [0.81] 0.81	0.79 [0.85] 0.88	P=0.92	P=0.87	P=0.11
PW, cm	0.77 [0.86] 0.85	0.76 [0.96] 1.1	P=0.59	0.76 [0.88] 0.94	0.71 [0.88] 0.99	P=0.69	P=0.84	P=0.48
HR	94 [109] 119	93 [103] 117	P=0.14	91 [96] 102	95 [97] 100	P=0.90	P=0.13	P=0.43

The echocardiographic data were analyzed by the generalized least squares model to account for correlation within animals. Data are presented as lower quartiles [mean] upper quartiles. FS indicates fractional shortening; HR, heart rate; IVS, interventricular septal wall thickness in cm; LVIDd and s, left ventricular inner diameter, diastole and systole in cm; PW, posterior wall thickness in cm.

Assessment of Cardiac Fibrosis

Fibrosis in LV myocardium remote from the infarct was measured by Masson's trichrome staining of sections as previously described[6] and by measurement of hydroxyproline content from frozen myocardium dried overnight at 60°C, using a commercial assay system from Sigma Aldrich per manufacturer's instructions. Myocyte short axis cross-sectional area was measured using ImageJ analysis of appropriately oriented myocytes in photomicrographs of trichrome or hematoxylin and eosin stained sections in the left ventricular myocardium remote from the infarct. At least 50 myocytes were measured per animal.

Table 3. Hemodynamic Measurements & Tissue Weight Ratios

Parameter	Treated (n=8)	Untreated (n=5)	Test Statistic
SV, mL	150 [161] 184	102 [107] 107	P=0.15
LVEDV, mL	200 [234] 269	235 [251] 327	P=0.40
LVESV, mL	45 [72] 88	47 [143] 224	P=0.26
LVEF, %	62 [71] 80	32 [45] 42	P=0.033
SPB, mm Hg	81 [84] 96	76 [81] 96	P=0.86
Baseline LVEDP, mm Hg	2.9 [4.8] 5.8	1.0 [4.8] 5.9	P=0.784
Baseline HR, bpm	85 [89] 93	72 [79] 81	P=0.108
Heart/body weight	4.58 [4.79] 5.13	3.6 [4.06] 4.16	P=0.077
Lung W/D	2.60 [2.93] 3.20	3.11 [3.35] 3.48	P=0.15

The Wilcoxon rank sum test was used to analyze cardiac function parameters and tissue ratios. The results are summarized as lower quartiles [mean] upper quartiles and the corresponding test statistic. Heart/body weight indicates heart to body weight ratio; HR, heart rate; Lung W/D, lung wet to dry ratio; LVEDP, left ventricular diastolic pressure; LVEDV, left ventricular end diastolic volume; LVEF, left ventricular ejection fraction; LVESV, left ventricular end systolic volume; SBP, systolic blood pressure; SV, stroke volume.
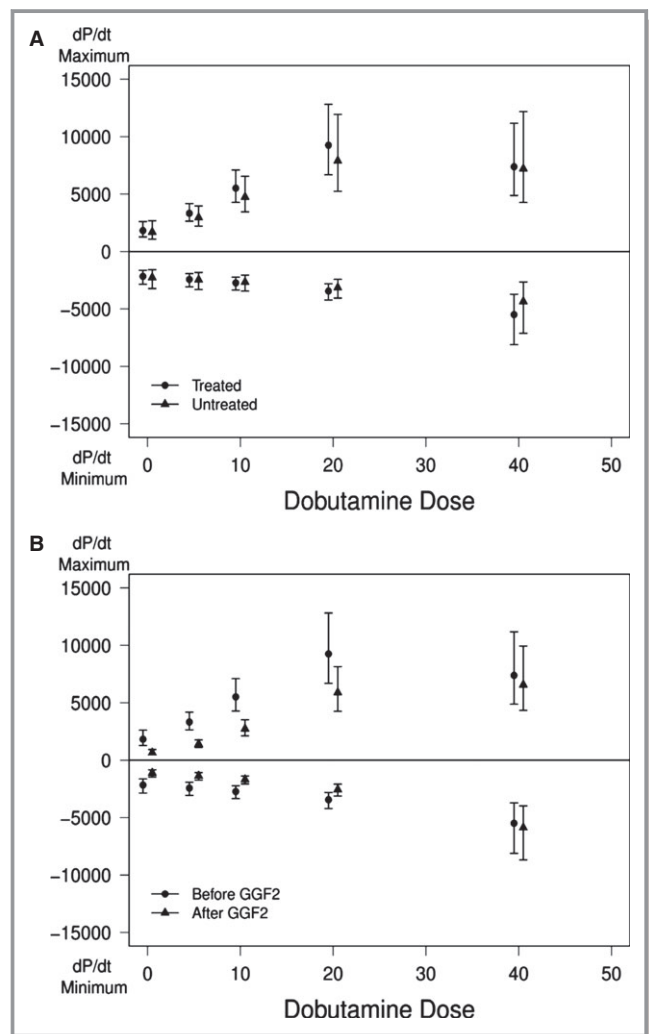

Figure 2. Effect of NRG-1β on left ventricular contractility and dobutamine reserve is shown. Chronic NRG-1β treatment (A) did not alter baseline dP/dt maximum and minimum or dobutamine responses. Acute NRG-1β treatment (B) reduced baseline dP/dt maximum and minimum as well as response to low dose dobutamine. Statistical results are shown in Table 4. GGF2 indicates glial growth factor 2; NRG-1β, neuregulin-1β.

Electron Microscopy

Prior to electron microscopy, left ventricular tissue was fixed in 4% glutaraldehyde in a 0.1 mol/L phosphate buffer solution and stored at 4°C. For transmission electron microscopy (TEM), samples were post-fixed with 1.0% osmium tetroxide, epoxy-embedded, and sectioned to ≈70 nm thickness. Sections were post-stained with 2.0% uranyl acetate and Reynolds lead citrate. Sections were analyzed using a Philips/FEI T-12 Transmission Electron Microscope at an accelerating voltage of 80 kV by an investigator (CG) blinded to treatment group. Tissue handling post-fixation and image collection was completed at the Vanderbilt Cell Imaging Shared Resource (CISR). Images were acquired using a Philips/FEI T-12 TEM.

For scanning electron microscopy (SEM), glutaraldehyde-fixed tissues were macerated prior to processing for SEM, samples were macerated using a modified method previously published. Briefly, samples (≈2000 mm^3 in size each) were incubated in 10% aqueous NaOH at room temperature for 10 days. In our hands, initial storage of samples in 4% glutaraldehyde was required to generate samples of sufficient size and quality to subsequently process. Fresh or frozen samples disintegrated using this method. After maceration, tissues were rinsed in distilled water until transparent and then incubated in 1% tannic acid for 4 hours at room temperature. Samples were then rinsed in distilled water overnight and then further processed in the Cell Imaging Shared Resource (CISR) microscopy core at Vanderbilt, as follows: Samples were rinsed 3 times in 0.1 mol/L sodium cacodylate buffer with 1% calcium chloride and transferred into 1% osmium tetroxide in the same buffer solution. Samples were again rinsed 3 times in the buffer, and then dehydrated through a graded series of aqueous solutions of ethanol, ending with 3 exchanges of pure ethanol. Samples were transferred into the EMS 850 critical point dryer (CPD) in pure ethanol. Ethanol was substituted with liquid carbon dioxide in the CPD. Samples were dried at the critical point for carbon dioxide.

Samples were removed from the CPD and mounted on SEM stubs with carbon adhesive tabs and colloidal silver paint. Samples were sputter coated with gold/palladium alloy in the Cressington 108 sputter coater. Image data was collected in the FEI Quanta 250 field emission gun scanning electron microscope (FEG SEM) of the Cell Imaging Shared Resource (CISR) at Vanderbilt University Medical Center. The FEG SEM was operated in high-vacuum mode, at an accelerating voltage of 8 or 10 kV.

Western Blot Analysis

Swine LV heart samples collected from areas remote from the site of infarct were stored at −80°C until needed. For protein analysis, samples were homogenized in RIPA buffer (Millipore), supplemented with protease and phosphatase inhibitors (Thermo Scientific), passed through syringes at least 5 times, centrifuged at 8000g for 10 minutes, and the supernatants collected for SDS polyacrylamide gel electrophoresis. Protein samples (30 μg/lane) were mixed with Lamaellie loading buffer (Bio-Rad) with β-mercaptoethanol added, run in a 1× solution of running buffer (Bio-Rad) at 100 V for 1 to 2 hours and then transferred to PVD membrane. Membranes

Table 4. Estimated Lowest Quartile, Mean, and Upper Quartile Maximum and Minimum dP/dt at Each Dobutamine Dose Before and After Acute NRG-1β, and Test Statistic for Comparison (Data Shown Graphically in Figure 2)

| Dose	Before Infarction			After Infarction			P Value
	XXX	XXX	XXX	XXX	XXX	XXX	
dP/dT maximum, mm Hg/ms							
0	1273	1823	2610	454	651	932	7.0e-05
5	2644	3324	4181	1119	1407	1769	2.0e-07
10	4282	5515	7104	2121	2732	3520	1.2e-04
20	6688	9259	12 818	4256	5892	8157	5.4e-02
40	4881	7386	11 175	4342	6570	9941	7.0e-01
dP/dT minimum, mm Hg/ms							
0	−1635	−2163	−2861	−839	−1110	−1469	0.00096
5	−1921	−2430	−3074	−1081	−1367	−1730	0.00070
10	−2227	−2731	−3347	−1374	−1684	−2064	0.00100
20	−2812	−3447	−4226	−2084	−2554	−3131	0.04137
40	−3720	−5495	−8115	−3980	−5878	−8682	0.81047
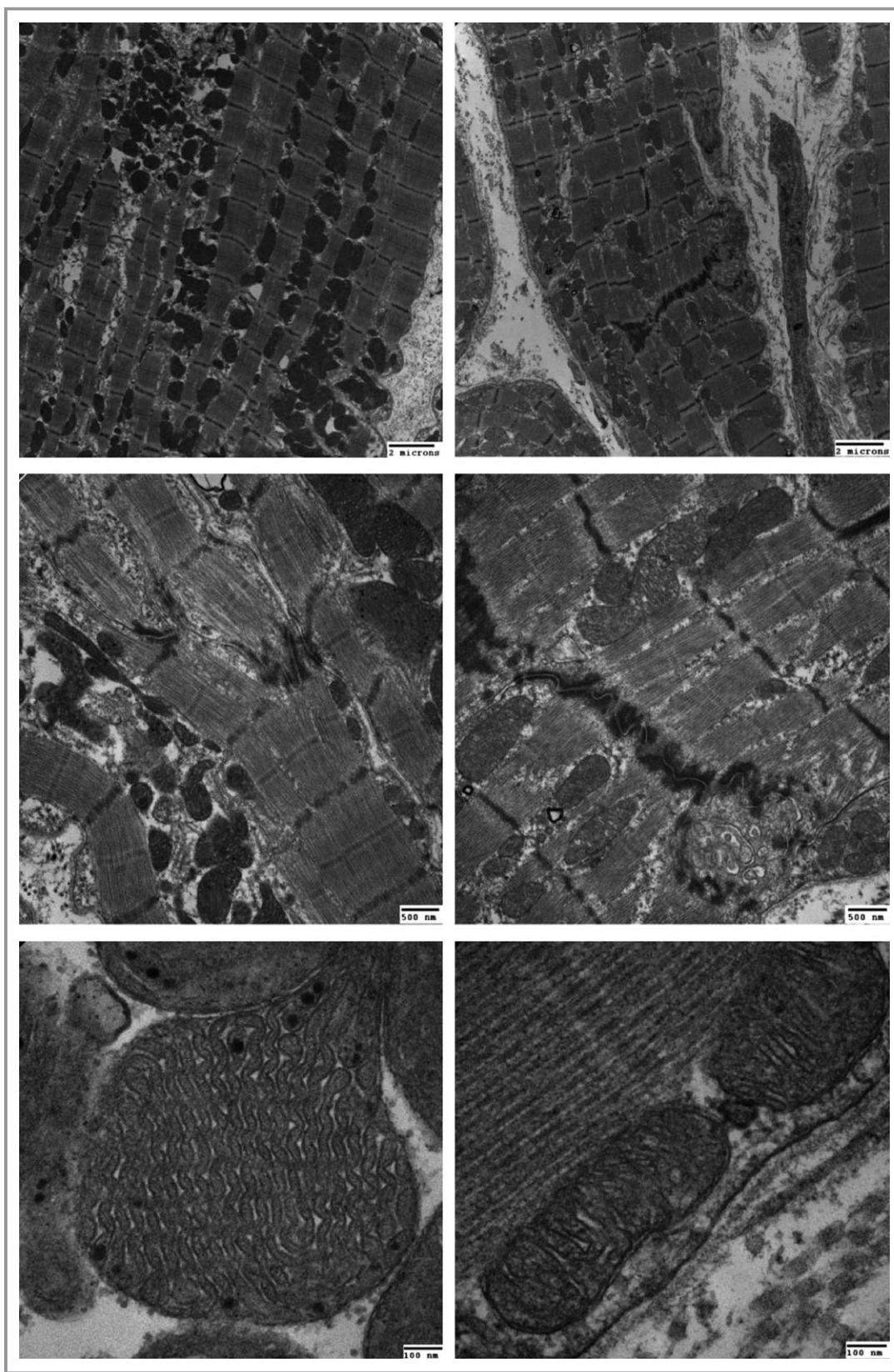
Figure 3. Representative TEM images of untreated (left) and GGF2 treated (right) swine (n=5) are shown. The first row (×6500) displays a low magnification view of sarcomeric structure. The second row (×22 000) highlights differences in intercalated disc structure, while the third (×110 000) shows mitochondrial abnormalities, including swollen morphology, bloated cristae and numerous mitochondrial granules, in untreated animals. GGF2 indicates glial growth factor 2; TEM, transmission electron microscopy.

were rinsed in TBS, blocked in 5% milk (in TBST) for 1 hour at room temperature, washed in TBST 3 times (15 minutes each). Primary antibody purchased from Santa Cruz (rabbit anti-ErbB3) was diluted 1:1000 in TBST with 5% BSA added and incubated overnight at 4°C. The membrane was then washed in TBST 3 times (15 minutes each). The membrane was subsequently incubated in HRP-linked goat anti-rabbit (Santa Cruz), diluted 1:2000 in 5% milk-TBST for 1 hour at room temperature. Membranes were again washed, followed by incubation in chemiluminescence (Pierce), exposure to X-ray film, and development using standard X-ray film in a dark room.

Isolation of Mouse Cardiac Fibroblasts

As previously described,[10] hearts from three 8- to 10-week-old C57Bl6 mice (Jackson Laboratories) were dissected to

Table 5. Functional Analysis of NRG-1β-Induced Transcriptional Changes

Functional Category	No. of Genes	P Value
Molecular and cellular functions		
Cellular growth and proliferation	116	4.8×10^{-11}
Cell death	108	6.8×10^{-10}
Cell cycle	73	3.8×10^{-9}
Cellular movement	76	1.4×10^{-8}
Cellular development	88	8.8×10^{-7}
Physiological system development and function		
Tissue development	82	2.6×10^{-7}
Connective tissue development and function	54	8.8×10^{-7}
Nervous system development and function	42	5.9×10^{-6}
Cardiovascular system development and function	34	1.1×10^{-4}
Embryonic development	59	1.1×10^{-4}
Top transcription factors		
TP53 (Affected)	29	5.9×10^{-10}
AHR (activated, z score=2.665)	12	6.9×10^{-6}
ACTB (inhibited, z score=−2.000)	4	8.0×10^{-5}
Top NRG-1β -induced transcripts		
FOSB (18.5), AREG/AREGB (12.4), NR4A2 (10.0), IFRD1 (9.7), KLF5 (6.7), FAM46A (5.4), TRIB1 (5.4), FOS (5.0), plk2 (4.4), IER5 (4.3)		
Top NRG-1β-depressed transcripts		
C1QTNF3 (−7.9), ZNF367 (−7.5), HBB (−5.9), HBA1/2 (−5.9), POSTN (−5.5), PBK (−5.2), LMO4 (−4.5), SERPINB13 (−4.4), RACGAP1 (−4.2), ZNF436 (−3.8)		

ACTB indicates beta actin; AHR, aryl hydrocarbon receptor; NRG-1β, neuregulin-1β.
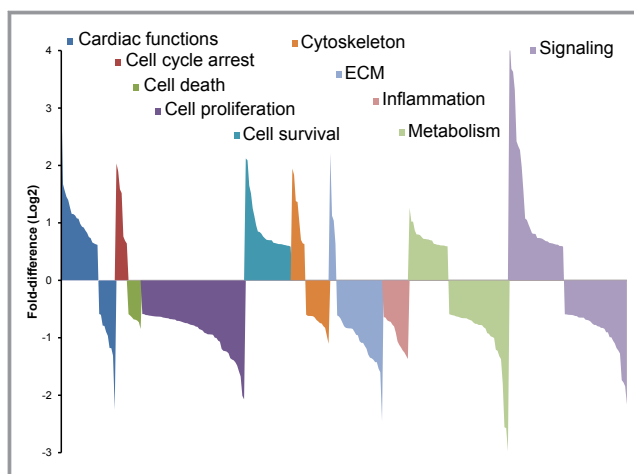

Figure 4. Area chart showing log2 fold-differences for glial growth factor 2-treated pigs, compared to untreated control animals. Genes are grouped by function and colored accordingly. The vertical axis indicates the relative change (up or down), and the horizontal represents individual genes found as significantly differential by the amount shown. Functional categories were assigned based on a combination of enriched biological processes identified by functional analysis and information available in NCBI Entrez Gene, Genecards, Aceview, and Pubmed databases. ECM indicates extracellular matrix.

isolate ventricular tissue, which was then minced and incubated with 10 mL of digestion solution (10 mg/mL collagenase II, 2.5 U/mL dispase II, 1 µg/mL DNase I, and 2.5 mmol/L $CaCl_2$) for 20 minutes at 37°C. A filtered myocyte-free single-cell suspension in PBS containing 0.5%

Table 6. Quantitative RT-PCR Confirmation of Gene Expression Results

	Low		High	
	Array	RT	Array	RT
Col1a2	−1.1	−1.6	−2.7	−1.6
Col3a1	nc	nc	−2.1	−1.7
Col4a1	−1.1	−3.4	−1.6	−2.1
Col5a2	nc	nc	−2.5	−1.5
Col12a1	−1.2	−1.4	−2.1	−1.5
Gadd45B	nc	nc	3.6	2.0
MyoCd	nc	nc	2.6	1.6
FosB	1.3	2.8	18.5	8.0
Nr2a4	1.4	3.3	10.0	25.5
Areg	1.6	1.8	12.4	3.4
KLF5	3.9	1.9	6.7	5.5

Fold-differences (NRG-1β-treated/untreated) for selected genes (first column) that were determined to be significantly altered based on microarrays (Array) were verified by quantitative RT-PCR (RT). Results for low and high dose NRG-1β are shown. A negative sign ("−") before the number indicates down-regulation in NRG-1β-treated animals, relative to untreated controls. NRG-1β indicates neuregulin-1β.

BSA and 2 mmol/L EDTA (PBS/BSA/EDTA) was treated with mouse BD Fc Block (clone 2.4G; BD Biosciences), and immune cells were magnetically removed with CD45 microbeads (Miltenyi Biotec Inc). CD45-depleted cell suspension was incubation with phycoerythrin (PE)-conjugated CD31 (clone 390; eBioscience) and allophycocyanin (APC) -conjugated CD105 (clone MJ7/19; Biolegend) antibodies. CD31$^+$ endothelial cells were removed using anti-PE microbeads (Miltenyi Biotec) and CD105$^+$ cardiac fibroblasts were magnetically isolated with anti-APC microbeads (Miltenyi Biotec) from the flow-through CD31$^-$-negative cells. Primary cardiac fibroblasts (CD105$^+$CD31$^-$CD45$^-$) were plated at a density of 2×10^7 cells/mm^2 and cultured in DMEM supplemented with 10% FBS, 100 IU/mL penicillin, 0.1 mg/mL streptomycin, and 2 mmol/L glutamine under a humidified atmosphere of air/CO$_2$ (19:1) at 37°C.

Isolation and Growth of Rat Cardiac Fibroblasts

Hearts from 6- to 7-week-old male Sprague–Dawley SD rats (Jackson Laboratories) were isolated by retrograde perfusion to obtain supernatants for fibroblasts, as previously described.[11] The Langendorff-perfusion apparatus was prepared by running hot water through the tubing for 10 minutes, followed by Tyrode's Ca^{2+} solution (137 mmol/L NaCl, 5.4 mmol/L KCl, 1.2 CaCl$_2\times2$H$_2$O, 0.5 mmol/L MgCl$_2$, 10 mmol/L HEPES, 10 mmol/L glucose) for 2 minutes. After isoflurane anaesthetization, the rat heart was excised, placed in KB buffer (85 mmol/L KOH, 30 mmol/L KCl, 30 mmol/L KH$_2$PO$_4$, 3 mmol/L MgSO$_4$, 0.5 mmol/L EGTA, 10 mmol/L HEPES, 50 mmol/L L-glutamic acid, 20 mmol/L taurine, 10 mmol/L glucose), and then clamped and tied to the Langendorff apparatus. The heart was
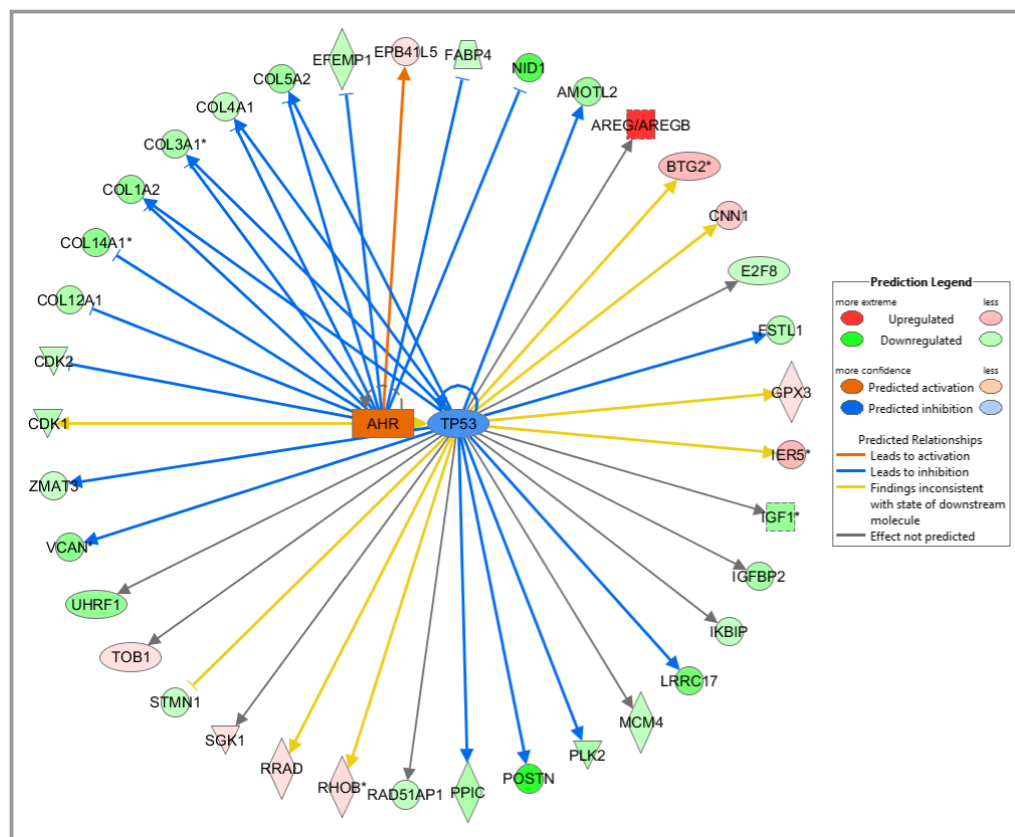

Figure 5. Results of transcription factor analysis using Ingenuity Pathway Analysis software program for NRG-1β treatment-induced gene expression changes observed in post-MI swine. Based on this analysis of observed gene expression alterations, AHR (aryl hydrocarbon receptor) activity was predicted to be activated (center, orange square). Conversely, TGFbeta (TGFbeta shown in blue) was predicted to be inhibited. Genes regulated by AHR and/or TGFbeta that were altered in expression based on microarrays are shown on the periphery and colored according to level of alteration. Up-regulated genes are colored in various shades of pink to red, with darker indicating higher magnification of change. Similarly, down-regulated genes are shown in light to dark green, the latter indicating a greater magnitude of inhibition compared to lighter shades. Figure produced using Ingenuity Pathway Analysis program (Qiagen). MI indicates myocardial infarction; NRG-1β, neuregulin-1β.

perfused with Tyrode's Ca^{2+} solution at a flow rate of 20 for ≈1 minutes (or until blood was completely removed). The heart was then perfused with Tyrode's Ca^{2+}-free solution (135 mmol/L NaCl, 4 mmol/L KCl, 1 mmol/L $MgCl_2$, 0.33 mmol/L $NaH_2PO_4 \times 2H_2O$, 10 mmol/L HEPES, 10 mmol/L Glucose) for 5 to 10 minutes until contractions stopped and heart size increased. Enzyme solution (15 mg non-specific protease and 55 mg of 300 U/mg collagenase in 75 mL Tyrode's Ca^{2+}-free buffer) was subsequently perfused through the heart for 20 minutes, followed by KB buffer for 5 minutes. The heart was further processed and cells filtered to produce fibroblast-containing supernatant, which was centrifuged for 15 minutes at 850g. After spinning down, the supernatant was aspirated and the pellets suspended in 15 mL of growth medium (500 mL Gibco DMEM, 7% FBS, 1% penicillin streptomycin).

Flow Cytometric Analysis of α Smooth Muscle Actin (αSMA) Expression

Flow cytometry was performed as previously described.[10] Briefly, primary cardiac fibroblasts ($CD105^+CD31^-CD45^-$) from passage 1 were cultured in 10% FBS DMEM in the absence or presence of 30 ng/mL of Neuregulin-1β for 48 hours. Cells were trypsinized, washed with PBS and resuspended in PBS/0.5% BSA/2 mmol/L EDTA buffer containing murine Fc block reagent (BD Biosciences). The cells were then incubated with CD105-APC (clone MJ7/19; Biolegend) antibody for 20 minutes at 4°C, washed once with 10 volumes of cold PBS/BSA/EDTA, fixed and permeabilized using 4% paraformaldehyde and 0.1% saponin in Ca/Mg free DPBS. Cells were stained with fluorescein isothiocyanate (FITC)-conjugated anti-αSMA (Clone 1A4, Sigma) antibody for 25 minutes at 4°C. Mouse FITC-conjugate IgG2a (Clone UPC-10, Sigma) were used as an isotype control. Viable and nonviable cells were distinguished using LIVE/DEAD Fixable Blue Stain kit (Invitrogen). Data acquisition was performed using an LSRII flow cytometer (BD Biosciences), and the data were analyzed with WinList 5.0 software (Verity Software House, Inc). Antigen negativity was defined as having the same fluorescent intensity as the isotype control.

Statistical Analysis

Statistical analyses of echocardiography and dobutamine challenge data were performed using the generalized least squares method using compound symmetry structure. This linear regression model accounts for correlation within animals and was used to investigate whether GGF2 treatment affected the 35-day outcomes (fractional shortening [FS %]), LV inner diameter at diastole (LVIDd), and other echocardio-

graphic measures. Estimated mean values were fit using restricted maximum likelihood or REML and are shown with 95% confidence intervals.

Analysis of intraventricular hemodynamics data was performed using the generalized least square method and the Wilcoxon rank sum test. The GLS regression model was fit to investigate the dose effect of dobutamine on the 1st derivative or rate of change of ventricular pressure ($\pm$dP/dt). Non-linearity was addressed by applying tail-restricted cubic splines with 3 knots to dose variable, and transformation was applied when the normality assumption did not hold. Predicted mean values were fit using REML and are shown with its 95% confidence interval. SV, EDV, ESV, LVEF%, LVEDP, and heart rate were analyzed using the Wilcoxon rank sum test. The Wilcoxon rank sum test was performed for comparison of continuous variables and summarized as medians, upper quartiles, and lower quartiles.

Statistical analysis of microarray data was performed as previously described.[6] For analysis of in vitro experiments, results were statistical analysis was performed using Student t test or ANOVA with Bonferroni correction for multiple comparisons as indicated.
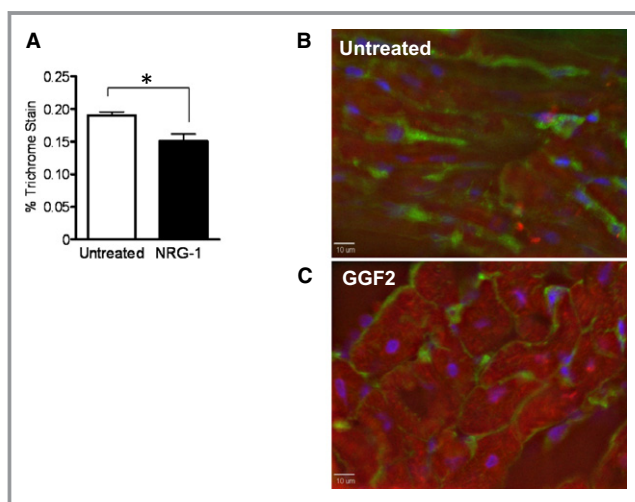

Figure 6. A. Graphical representation of percent fibrosis in swine ventricular samples collected remote from the site of infarct. Error bars represent the standard error of the mean ($\pm$SEM) calculated from 3 untreated control animals and a total of 6 GGF2-treated animals. (*P=0.006 by t test). B and C, Representative immunohistochemistry of untreated (B) and GGF2-treated (C) left ventricular tissues, collected from post-MI swine, remote from the site of infarction. After fixation, tissues were stained with DAPI (blue), phalloidin (red) and anti-collagen IV (green). As shown, Collagen IV was more evenly spaced and thinner in GGF2-treated animals, compared to untreated control pigs. Scale bar represents 10 μm. DAPI indicates 4',6-diamidino-2-phenylindole; GGF2, glial growth factor 2; MI, myocardial infarction; NRG-1β, neuregulin-1β.
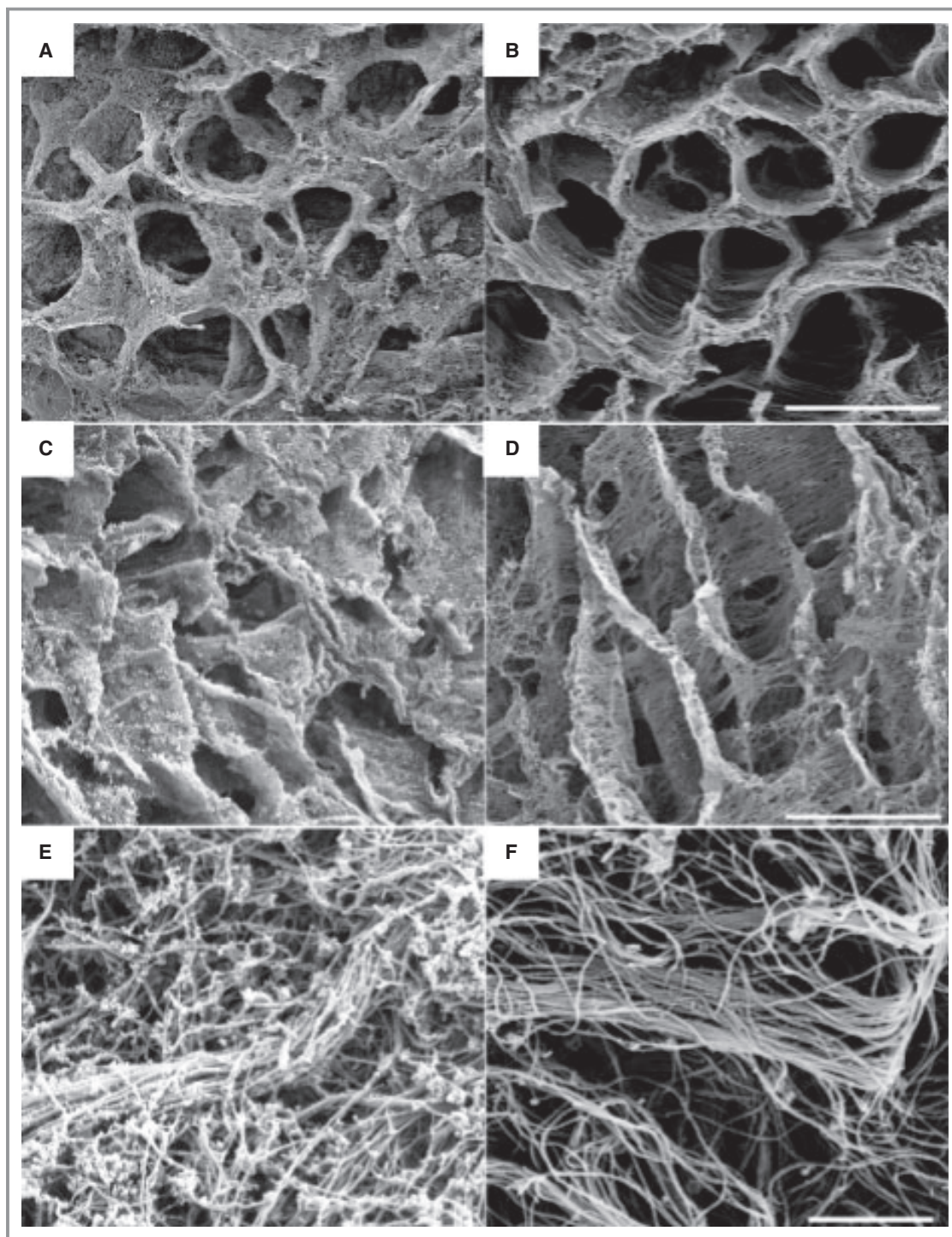
Figure 7. Representative scanning electron micrographs of the 3-dimensional arrangement of LV extracellular matrix in untreated and GGF2-treated pigs, after NaOH maceration. The top 2 panels show the matrix in cross section, with a typical honey-comb structure that is thicker and less regular in untreated pigs (A), compared to GGF2-treated animals (B). Middle panels show the matrix in longitude, which highlights the regular spatial arrangement of fibers in GGF2-treated pigs (D), Conversely, untreated animals exhibited a thick, matte-like matrix, as shown in the (C). Higher magnification revealed a very different ultrastructure of matrix fibers between treated and untreated animals. Cardiac matrix fibers of untreated pigs contained many proteinaceous "flake"-like nodules along the longer collagen bundles (E), as compared to GGF2-treated animals, which exhibited more spacing between fibers that contained very few of these nodule-like attachments (F). Bars=40 μmol/L (A through D) and 2 μmol/L (E and F). GGF2 indicates glial growth factor 2; LV, left ventricular.

Results

GGF2 Treatment Alters Post-MI Left Ventricular Remodeling

Thirteen of 23 swine survived acute infarction and completed the study, 5 untreated and 8 treated, which is similar to post-MI survival rates for other studies in swine.[7] Pretreatment echocardiographic measurements of LVIDd, LVIDs, and FS were acquired at 1 week post-MI and subsequently at 5 weeks post-MI (Figure 1, Table 2). Baseline measures were similar between groups, while biweekly GGF2 treatments for

4 weeks was associated with improved FS% (P=0.019) and reduced LVIDd (P=0.003) compared with untreated animals. Untreated animals demonstrated progressive remodeling as evidenced by an increase in LVIDd from day 7 to 35 (P=0.0003), and decline in FS% (P=0.002). In contrast, GGF2 treated animals showed no increase in LVIDd (P=0.41), with improved FS% (P=0.04). GGF2 was associated with an increase in LV interventricular septal thickness (P=0.04), though there was no increase in posterior wall thickness (P=0.59), thus, GGF2 treatment prevented LV dilation and improved left ventricular systolic function in post-MI swine.
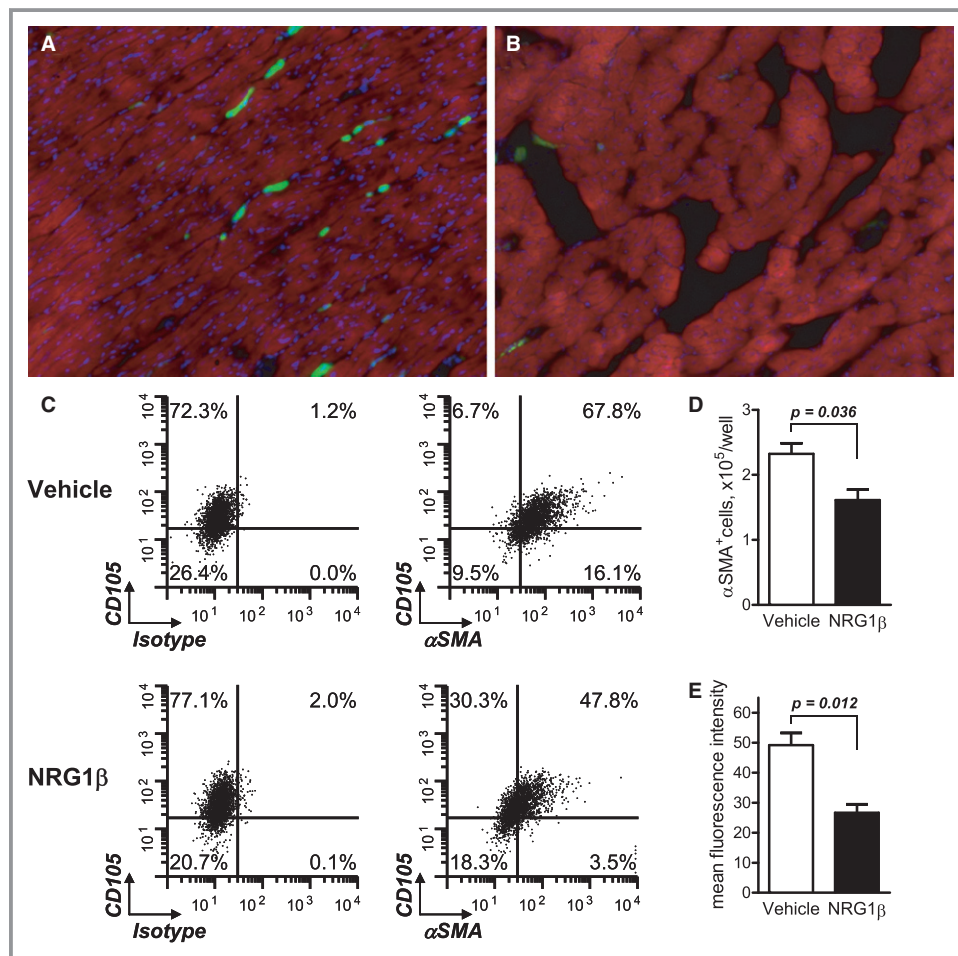

Figure 8. Representative immunohistochemistry of swine LV tissues from untreated (A) and GGF2-treated (B) post-MI pigs. Tissues were stained with DAPI (blue), phalloidin (red), and anti-αSMA (green). C, Representative cytofluorographic dot plots showing the percentage of αSMA+ fibroblasts incubated in the absence (*vehicle, upper panel*) or presence of 30 ng/mL NRG-1β (*lower panel*) for 48 hours; (D) Graphic representation of data from flow cytometric analysis of αSMA expression in cardiac fibroblasts incubated in the absence (*vehicle, open bar*) or presence of 30 ng/mL NRG-1β (*closed bar*) for 48 hours. Number of αSMA+ cells was calculated from percentage of αSMA-expressing and total number of cells; E, Mean fluorescence intensity of αSMA expression in cardiac fibroblasts as assessed by flow cytometry. Data represent mean±SEM from 3 independent experiments. *P*-values indicate significance level calculated by t test. GGF2 indicates glial growth factor 2; LV, left ventricular; MI, myocardial infarction; NRG-1β, neuregulin-1β; αSMA, α smooth muscle.

Assessment of Left Ventricular Volume, Contractility and Dobutamine Response

Hemodynamic assessment of systolic and diastolic function by Millar® conductance catheter at 35 days post-MI (HR, SBP, LVEDP, SV, LVEDV, LVESV, Table 3) were not different between groups. However, LVEF% (LVEDV−LVESV/LVEDV) was higher in the treated group (*P*=0.033, Figure 1C). There was no difference in baseline dP/dt maximum and minimum between animals treated for 4 weeks with NRG-1β and untreated animals (Figure 2A). Chronic GGF2 treatment also did not change the contractile response to dobutamine.

To assess effects of an acute challenge of GGF2 on cardiac contractility after 4 weeks of treatment, a single dose (2 mg/kg) was administered and hemodynamics were recorded at baseline and the response to dobutamine was reassessed (Table 4). An acute GGF2 challenge reduced dP/dt maximum and minimum, as well as blunted contractile response to dobutamine infusion (Figure 2B). GGF2 administration had no effect on heart rate at baseline or in response to dobutamine infusion (data not shown).

Myocardial and Tissue Responses to GGF2

Heart weight/body ratios were generally higher in treated swine (*P*=0.077), while lung wet/dry ratios tended to be lower (*P*=0.15, Table 3). No obvious differences were seen in left ventricular sections stained by H&E, and myocyte cross-sectional area was similar between untreated and treated (430±92 versus 436±107 μmol/L^2). However, ventricular ultrastructures were different when assessed by TEM (Figure 3). Intercalated discs were more difficult to locate and severely disrupted in untreated swine LV samples compared with those in GGF2-treated swine, which were generally abundant and well defined. In addition, there were many morphologically abnormal mitochondria in untreated swine that were not found in treated animals.

GGF2 Treatment Alters Global Gene Expression Profiles in Post-MI Swine

Left ventricular tissue remote from the site of infarct was collected from each of 8 animals (3 untreated controls, 5 GGF2-treated) and global gene expression assessed using microarrays. Analysis yielded 528 statistically significant probes (fold-difference ≥1.5, ANOVA *P* value ≤0.05) among the 3 groups of animals, including 245 characterized swine genes and 283 transcripts that did not include curated gene information. To characterize these differential transcripts, each probe source sequence was manually searched against the human reference genome using the UCSC Genome
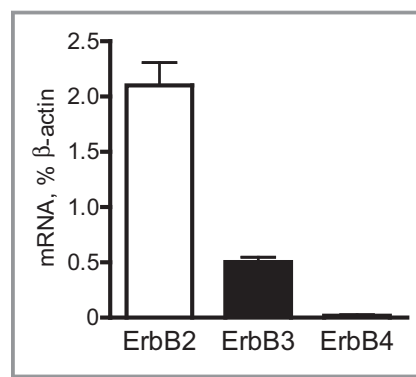

Figure 9. Graphical representation of ErbB receptor mRNA levels in flow-sorted primary mouse cardiac fibroblasts, relative to β-actin, as assessed by qRT-PCR. qRT-PCR indicates quantitative reverse transcriptase-polymerase chain reaction.

Bioinformatics' tool, BLAT. This analysis yielded an additional 172 orthologous human transcripts, representing 157 unique genes (Table S1).

GGF2 Treatment Down-Regulates Expression of Extracellular Matrix Transcripts

Based on functional analysis using Ingenuity Pathway Analysis software, enriched functions included cellular growth and proliferation, cell death, cell cycle, cell movement, and cellular development (Table 5). When differential genes were grouped by function (Figure 4), a clear pattern emerged showing that GGF2 up-regulated genes encoding cell cycle arrest and cell survival proteins, while depressing transcripts involved in cell proliferation and cell death. A notable finding was alteration of genes encoding ECM and matricellular proteins, which were almost exclusively down-regulated (Figure 4). These included 9 collagens (*COL1a2* [−2.7-fold], *COL3a1* [−1.9-fold], *COL4a1* [−1.6-fold], *COL5a2* [−2.5-fold], *COL8a1* [−2.1-fold],
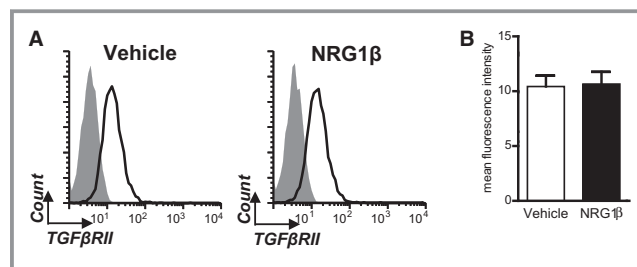

Figure 10. A. Representative flow cytometric histograms showing cell surface expression of TGFβRII in the absence (*vehicle*) or presence of 30 ng/mL neuregulin-1β (NRG1β). Gray-shaded histograms represent isotype-matched control and open histograms are specific anti-Tgfbr2 antibody. B, Mean fluorescence intensity of TGFβRII. Data represent mean±SEM from 4 independent experiments. TGFβRII indicates transforming growth factor beta receptor 2.
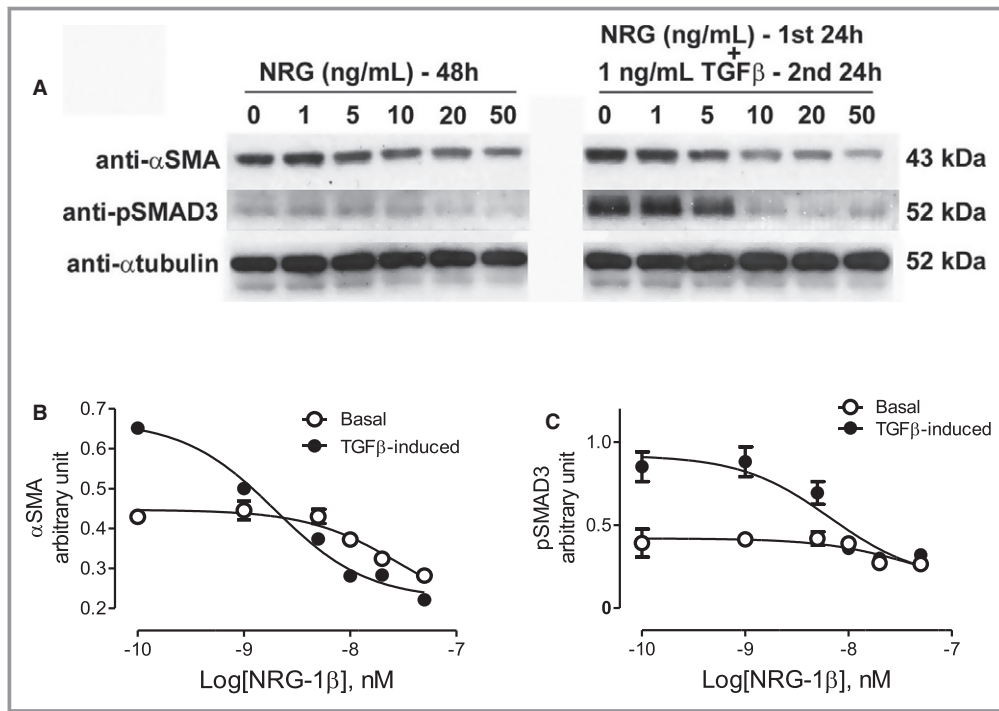
Figure 11. A. Representative Western blot analysis of NRG-1β–treated rat cardiac fibroblasts treated with 50 ng/mL of recombinant NRG-1β at various doses for 48 hours (lanes 1 to 6), 1 ng/mL TGFβ for 48 hours (lane 7) or with NRG-1β for 24 hours followed by 1 ng/mL TGFβ or 24 hours (lanes 8 to 13) and probed with anti-α-smooth muscle actin (αSMA) or phospho-SMAD3 (pSMAD3). B and C, Graph of Western blot analyses for αSMA and pSMAD3, respectively. NRG-1β inhibited basal and TGFβ induced αSMA at all concentrations ($P<0.0001$, ANOVA), and basal αSMA expression at concentrations of 10 ng/mL and above (P,0.001, ANOVA). NRG-1β inhibited basal and TGFβ induced pSMAD3 at concentrations of 10 ng/mL and above ($P<0.0001$, ANOVA), without any effect on basal pSMAD3. ANOVA indicates analysis of variance; NRG-1β, neuregulin-1β.

COL12a1 [−2.1-fold], *COL14a1* [−2.9-fold], *COL15a1* [−1.5-fold], and *COL21a1* [−2.3-fold]) and 17 matricellular proteins (eg, *SPARC, FBN1, NID1, POSTN* and *VCN*) (Table S1). Eleven genes were chosen for validation by real-time RT-PCR, the results of which confirmed GGF2-mediated regulation of these genes (Table 6).

Analysis to identify potential upstream regulators likewise suggested that post-MI GGF2 treatment inhibited ECM transcription. For example, TGFbeta-regulated transcripts were overrepresented, including 12 down-regulated genes (eg, 4 collagens, versican, and periostin). The aryl hydrocarbon receptor (AHR) was predicted to be activated (Z score=2.7) in response to GGF2 treatment (Table 5). Altered target genes known to be inhibited by AHR included 8 ECM genes (Figure 5) that were down-regulated in response to GGF2 treatment.

GGF2 Alters Fibrosis and Collagen IV Distribution

While left ventricle samples collected remotely from the infarct site in untreated pigs exhibited low levels of fibrosis

(0.19%), this was reduced when compared to animals that received GGF2 treatment post-injury, as measured by trichrome staining (P=0.006, Figure 6A). Consistent with this finding, there was a trend toward reduced hydroxyproline content in GGF2-treated tissues (0.47±0.03 µg/mg tissue) compared with untreated control animals (0.54±0.03 µg/mg tissue, P=0.065). One of the down-regulated collagens (collagen type IV) is a major perimysial structural protein that is readily visualized by immunohistochemistry. Ventricular tissue from GGF2-treated swine exhibited normal Collagen IV staining, enveloping individual myocyte bundles in a classic "honeycomb-like" pattern (Figure 6C, bottom panel). Regions of collagen IV staining in untreated control pig tissues, on the other hand, were thicker and less organized around cardiomyocytes (Figure 6C, top panel).

GGF2 Treatment Affects the Ultra-Structure of the Cardiac ECM

To examine ECM ultra-structure, we macerated swine tissues from both GGF2-treated and untreated animals in NaOH,
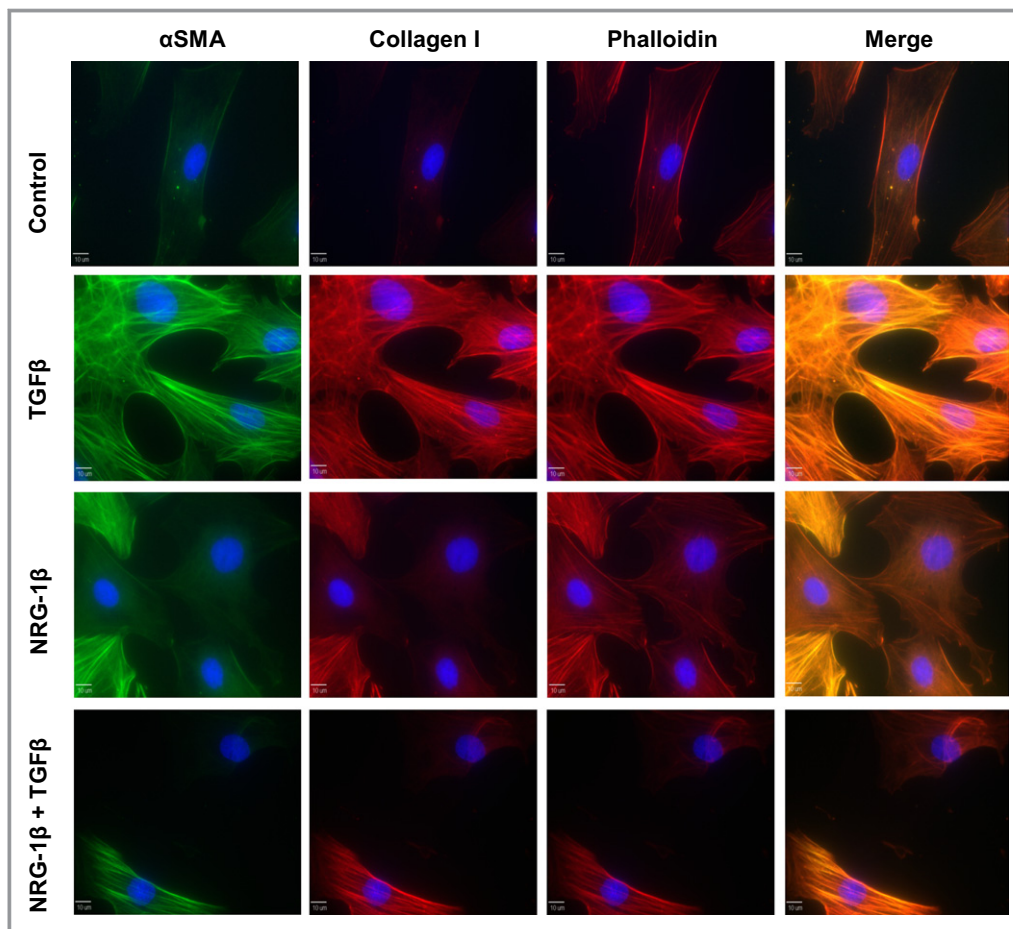
Figure 12. Immunohistochemistry of rat cardiac fibroblasts stimulated for 48 hours with TGFβ or NRG-1β (1 or 50 ng/mL, respectively) or pre-treated with 50 ng/mL NRG1-β for 24 hours before treatment with TGFβ (1 ng/mL for an additional 24 hours). After fixation, cells were stained with anti-αSMA to label myofibroblasts, anti-collagen I, phalloidin to stain actin filaments, and DAPI to visualize nuclei. Representative images of 3 independent experiments are shown. NRG-1β indicates neuregulin-1β; αSMA, α-smooth muscle actin.

which effectively eliminates all cellular material without disrupting the structure of the proteinaceous matrix.[12,13] Subsequent scanning electron microscopy (SEM) of processed samples revealed differences between GGF2-treated and untreated swine (Figure 7A and 7B). Cross-sections of treated ventricles displayed the typical honeycomb structure associated with non-diseased cardiac tissue; whereas these same structures were thicker, more densely packed, and less organized in untreated swine. There was a clear periodicity of fibers in GGF2-treated samples viewed on the long axis (Figure 7D) that was less obvious in untreated pigs (Figure 7C). Transverse sections of the ECM matrix from untreated controls were instead more mat-like in appearance, with little separation between individual proteinaceous fibers (Figure 7C). Closer inspection at a much higher magnification (Figure 7E and 7F) indicated that the fibers were very different in appearance, presumably due to differences in collagen

composition and/or post-translational processing and subsequent organization into 3-dimensional structures.

GGF2 Suppresses Myofibroblast (myoFb) Induction

GGF2 abrogation of pro-fibrotic gene expression and improvement in cardiac ECM structures could occur via regulation of cardiac fibroblasts. To assess this possibility, we performed immunohistochemistry using phalloidin, which stains actin fibers in both fibroblasts and myoFbs, and FITC-conjugated anti-smooth muscle actin, which is a marker for myoFbs but not fibroblasts. Ventricular tissue collected from GGF2-treated pigs exhibited fewer myoFbs than did tissues from untreated control animals (Figure 8).

We also examined whether GGF2/NRG-1β receptors are expressed in cardiac fibroblasts isolated from mouse heart by

Table 7. GGF2 Gene Expression Alterations Compared to Human Heart Disease

Study	Samples	n	Sig Genes	Common Genes
This study	Untreated	3	506	—
	NRG-1β	5		
E-TABM-480	Controls	4	1875	28
	Idiopathic	5		
GSE1145	Normal	15	4628	183
	Cardiomyopathy	92		
GSE1869	Unused donor	6	3469	109
	Pre-LVAD heart failure	31		
GSE5406	Non-failing	16	309	34
	Cardiomyopathy	194		
Total across human studies		363	7551	222

GGF2 indicates glial growth factor 2; LVAD, left ventricular assist device; NRG-1β, neuregulin-1β.

flow cytometry. Flow sorted mouse fibroblasts express high levels of ErbB2, moderate levels of ErbB3, and very little ErbB4 (Figure 9). To examine whether GGF2/NRG-1β directly acts on cardiac fibroblasts, we sorted single suspensions of mouse heart cells to isolate cardiac fibroblasts, cultured them for 6 days in the presence or absence of recombinant NRG-1β, and then measured the levels of fibroblasts versus myofibroblasts using flow cytometry. Forty-eight-hour treatment with NRG-1β (30 ng/mL) resulted in a lower percentage of myofibroblastss, as assessed by levels of α smooth muscle actin (αSMA), the most commonly used marker for distinguishing myofibroblastss from non-active fibroblasts (Figure 8C). This reduction was not due to a decrease in the cell surface expression of the receptor for TGFβ as measured by flow cytometry (Figure 10). NRG-1β also inhibited expression of αSMA protein as measured by Western blot analysis (Figure 11A and 11B) and immunohistochemistry (Figure 12) in rat cardiac fibroblasts with or without TGFβ stimulation. NRG-1β likewise reduced phosphorylation levels of the downstream TGFβ transcriptional effector SMAD3 (Figure 11A and 11C). While TGFβ treatment of rat cardiac fibroblasts induced classic myofibroblasts morphology, NRG-1β–treated cardiac fibroblasts exhibited a reduction in the active myofibroblast phenotype (Figure 12).

Discussion

Our main finding is that the recombinant GGF2 isoform of NRG-1β improved cardiac function in association with improved remodeling in a large animal model of post-MI heart failure. Chronic GGF2 treatment did not produce any adverse effects on diastolic function, and did not reduce beta-adrenergic responsiveness, which supports the further exploration of this growth and survival factor as a possible therapy for systolic heart failure. Analysis of gene expression led to our finding that GGF2 suppressed myocardial fibrosis. Consistent with a direct effect on remodeling, these observations provide additional mechanisms for the therapeutic effect of this cardiovascular growth factor.

Acute infusion of GGF2 lowered blood glucose in swine, which has not been reported in other species. NRG-1β is known to increase glucose uptake in cardiac myocytes, as well as skeletal muscle.[14,15] The hypoglycemic effect might therefore be expected, and may be more pronounced in swine specifically bred for rapid growth and overall mass of skeletal muscle. The hypoglycemic effect may explain the change in dobutamine responsiveness observed shortly after GGF2 infusion. It is also possible that GGF2 decreased dobutamine sensitivity by another mechanism, as the myocardium is able to maintain high-energy phosphate stores as well as myocardial function in the setting of hypoglycemia stimulated by insulin.[16] In cardiac muscle where metabolic substrate availability is controlled, NRG-1β reduces contractility by altering Ca^{2+} handling via NOS activation.[17]

Acute effects of recombinant NRGs on cardiac output may be further complicated by effects on systemic vascular resistance. Jabbour, et al studied the parenteral administration of the recombinant EGF-domain only fragment of NRG-1β in humans with stable heart failure and observed an increase in cardiac output in association with a 20% drop in systemic vascular resistance.[3] We did not measure systemic vascular resistance in the current study; however, we did not observe an effect of acute GGF2 infusion on end-systolic volume or systemic blood pressure, suggesting that there was no acute vasodilator effect of GGF2 in anesthetized post-MI swine. Further experimental work is needed simultaneously measuring myocardial contractility and vascular function as well as cardiac output to understand the acute effects of recombinant NRGs on cardiovascular function.

To identify the potential underlying mechanisms for GGF2/NRG-1β treatment, we examined tissue and cellular structure as well as global gene expression in GGF2-treated swine. NRG-1β is known to regulate myofilament formation,[18] mitochondrial function,[19] and focal adhesion formation at the intercalated disk,[20] all of which showed improved appearance in GGF2-treated swine. GGF2 normalization of mitochondrial structure is consistent with improved mitochondrial function reported in rodents treated with recombinant NRG-1β,[21] as well as changes in gene expression we observed in GGF2-treated rats.[6] A number of genes involved in regulation of growth were also over-represented in the microarray. It is possible that these relate to the increased LV septal wall thickness seen after treatment with GGF2, along

Table 8. Genes Altered in Human Heart Failure and NRG-1β-Treated Swine

Symbol	NRG-1β	Human	Function
COL14A1	−2.6	3.2	Regulation of fibrillogenesis, muscle development, important for growth and structural integrity of the myocardium[30,31]
COL15A1	−1.5	2.0	Member of the FACIT collagen family (fibril-associated collagens with interrupted helices) deficiency is associated with muscle and microvessel deterioration
COL1A2	−2.7	2.7	Fibril-forming collagen
COL21A1	−2.3	2.3	FACIT collagen
COL3A1	−1.9	2.5	Fibrillar collagen found in extensible connective tissues, frequently in association with type I collagen
CXCL12	−1.7	1.8	Also called SDF-1, sustained expression leads to increased fibrocyte recruitment,[32] cardioprotection, activation of cardiac stem cells[33]
DPT	−2.1	1.8	ECM protein, enhancement of TGF-beta activation, inhibits cell proliferation, accelerates collagen fibril formation, stabilizes collagen fibrils, expression increased in the infarct zone in rats after MI[34]
EFEMP1	−1.7	1.9	Member of the fibulin family of extracellular matrix glycoproteins, binds EGF receptor
ETFDH	1.5	1.5	Electron transfer flavoprotein
FBN1	−2.6	1.7	Large, ECM glycoprotein, structural component of calcium-binding microfibrils, heart development
HBB	−5.9	1.5	Regulation of blood pressure, blood vessel size
IQGAP2	−1.8	1.8	Regulation of actin cytoskeleton
LMOD2	1.7	1.6	Actin and tropomyosin binding, critical for sarcomere assembly[35]
LRRC17	−3.6	1.9	Osteoblast differentiation
LUM	−1.9	3.3	Binds to laminin, may regulate collagen fibril organization, expression level increased in the ischemic and reperfused rat heart[36]
MAP3K3	−1.6	1.8	Regulates SAPK/JNK and ERK pathways by activating SEK/JNK and MEK1/2, essential for early embryonic cardiovascular development (Yang), promotes TGF-beta-dependent epithelial to mesenchymal transformation[37]
MARCKS	−2.2	1.9	Filamentous (f) actin cross-linking protein and most prominent cellular substrate for PKC, binds calmodulin, actin, and synapsin, prevents myoblast migration[38]
NPR3*	−1.9	2.2	Regulation of blood pressure
PLSCR4	−2.2	2.0	Blood coagulation
POSTN	−5.5	2.0	Expression is induced by TGFβ following inflammation at the infarct border, leading to the production of type I collagen, also promotes collagen cross-link formation[39,40]
PROS1	−1.7	2.0	Inhibition of blood coagulation
RASL11B	−2.5	1.7	Closely related to the Ras branch of GTPases
SFXN1	−1.6	1.8	Iron transport
SPARC	−1.8	1.7	Matrix-associated protein, involved in ECM synthesis and promotion of changes to cell shape, regulates collagen interaction with cardiac fibroblast cell surfaces[41]; mediates early ECM remodeling after MI[42,43] mediates fibrosis[44–47]
ZBTB1	−1.6	2.1	Transcription factor that is essential for lymphocyte development
ZNF91	−1.8	1.5	Transcription regulation
ADAMTS1	2.2	−1.9	Heart trabecula formation, TGFβ activation, ECM remodeling
AREG	12.4	−1.6	Autocrine growth factor, fibroblast mitogen
BAG3	2.4	−1.5	Cell survival, regulation of angiogenesis, incorporated into the Z disc. Chaperone of HSP70
ELL2	3.8	−1.8	Regulation of transcription
FOS	5	−2.9	Transcription factor, downstream of SAPK/JNK
GADD45B	3.7	−1.6	Stress response, regulation of cell growth and survival
GPX3	1.8	−1.6	Detoxification of hydrogen peroxide
IFRD1	9.7	−1.6	Myoblast cell fate determination, adult somatic muscle development, muscle cell differentiation, stimulates muscle cell regeneration[48]
KLF5	6.7	−2.1	Promotes vascular smooth muscle cell proliferation, activates many genes inducible during cardiovascular remodeling[49]

Table 8. Continued

Symbol	NRG-1β	Human	Function
LNX1	2.2	−2.1	E3 ubiquitin ligase, targets interacting proteins for degradation through ubiquitination, interacts with ErbB2[50]
NR4A2	10	−2.7	Transcription factor, smooth muscle cell differentiation, regulation of muscle cell metabolism
PNP	1.5	−2.2	Enzyme responsible for formation of purine bases in DNA, crucial under energy-deprived conditions for the cell to metabolize adenosine during ATP degradation
RRAD	1.9	−2.0	Negative regulation of cell growth, inhibits cardiac fibrosis through connective tissue growth factor[51]
TBX5	2.2	−1.6	Heart development, contributes to cardiac repair through reprogramming resident cardiac fibroblasts[52]

EGF indicates epidermal growth factor; NRG-1β, neuregulin-1β.
*NPR3 was down-regulated in low dose NRG-1β-treated swine but up-regulated (2.2-fold) in swine that received the higher dose.

with the generally higher HW/BW ratios suggesting some degree of cardiac hypertrophy.

The GGF2-associated reduction in pro-fibrotic genes, including transcripts for ECM structural proteins (eg, collagens and fibrillins), matricellular proteins (eg, osteonectin, periostin, and versican), and myoFb markers was an unexpected finding. The novel effect of NRG-1β on cardiac fibroblasts in vitro and on ECM structure in vivo suggests that NRG-1β might prevent and/or reverse pathogenic remodeling in the heart. In conjunction with the down-regulation of ECM genes that are typically associated with the development and progression of fibrosis, the pro-fibrotic TGFβ signaling pathway was likely inhibited by GGF2/NRG-1β treatment, based on gene expression profiles of GGF2-treated swine and cardiac fibroblast cell culture experiments. For example, GGF2 increased transcriptional expression of RANBP3, which negatively regulates TGFβ signaling by mediating the nuclear export of SMAD transcription factors.[22] GGF2 also decreased expression of the gene encoding P311 protein, which induces TGFβ activation and conversion of fibroblasts to myoFbs.[23]

Further analysis of microarray results revealed a potential role for GGF2 in activation of AHR (aka dioxin receptor), an inducible transcription factor important for xenobiotic detoxification and other cellular stress responses. *Ahr* null mice develop cardiovascular disease,[24] liver dysfunction and fibrosis,[25] dermal fibrosis,[26] liver retinoid accumulation,[27] and shortened life span.[28] More recently, Lehmann et al reported AHR-mediated inhibition of TGFβ-induced trans-differentiation of human fibroblasts to myoFbs,[29] which is consistent with the observed decrease in cardiac tissue αSMA-expressing myoFbs in GGF2-treated swine.

We compared swine microarray data with several curated human cardiomyopathy data sets (Table 7), including a total

Table 9. Functional Analysis of Human Heart Failure Transcripts That Responded to NRG-1β Treatment in Post-Infarcted Swine

Gene Ontology	Count	B-H, *P* Value	Genes
Biological process			
Collagen fibril organization	5	5.3×10^{-4}	COL14A1, LUM, COL3A1, COL1A2, POSTN, DPT
Extracellular matrix organization	6	2.1×10^{-3}	
Extracellular structure organization	6	1.2×10^{-2}	
Cellular component			
Proteinaceous extracellular matrix	12	2.3×10^{-9}	COL21A1, LUM, FBN1, EFEMP1, COL3A1, COL15A1, POSTN, SPARC, CXCL12, COL14A1, GPX3, COL1A2, ADAMTS1, AREG, PROS1, DPT
Extracellular matrix	12	2.6×10^{-9}	
Extracellular region part	15	6.2×10^{-8}	
Extracellular matrix part	8	8.6×10^{-8}	
Collagen	5	1.4×10^{-5}	
Extracellular region	16	5.2×10^{-5}	
Fibrillar collagen	3	3.3×10^{-3}	
Molecular function			
Extracellular matrix structural constituent	6	3.7×10^{-4}	COL14A1, LUM, FBN1, COL3A1, COL1A2, COL15A1

NRG-1β indicates neuregulin-1β.

of 15 separate patient group versus control group comparisons. We found an overlap of 222 genes differentially expressed between normal and failing human hearts that were also transcriptionally altered in response to GGF2 treatment in the swine MI model (Table 8). These overlapping genes exhibited a statistically significant functional pattern related to the structure and organization of the ECM (Table 9). This suggests potential targets of GGF2/NRG-1β therapy in heart failure that might be useful as indicators of efficacy as the clinical development of NRG's proceeds.

Microarray results suggest additional signaling changes occur that may also contribute to the beneficial effects of GGF2 on cardiac structure and function. GGF2 treated swine heart showed increased expression of several cardioprotective genes, such as *KLF5,*[53] *CRYAB,*[54] and *PER2,*[55] while down-regulating transcripts associated with cardiac dysfunction (eg, *BNP* and *IL6ST*).[56,57] Alterations in expression of genes important for angiogenesis, blood pressure regulation, and coagulation were also observed. For example, the genes encoding coagulation factor V and thrombomodulin were both up-regulated in GGF2 treated swine (*F5*: 1.8-fold, *THBD*: 2-fold), while the *PLSCR4* gene, which encodes a phospholipid scramblase, and the gene encoding Protein S (*PROS1*) were down-regulated (-2.3-fold and -1.7-fold, respectively).

Several days of prolonged infusions of the EGF-domain only fragment of NRG-1β in humans with stable heart failure has persistent beneficial effects on cardiac function.[3,4] The finding that twice-weekly infusion of the GGF2 isoform of NRG-1β improves ventricular remodeling in swine suggests that prolonged infusions may not be necessary to achieve a benefit from this form of NRG-1β. Preliminary results of a phase 1, double-blind, placebo-controlled study of single ascending doses of GGF2 in patients with left ventricular dysfunction and symptomatic heart failure has recently been reported.[58] While subjects in this study received only a single dose of placebo or GGF2, the study was notable for trends of dose-related and long-lasting improvement in cardiac function. Further clinical studies are needed to define the reproducibility and durability of these effects, and whether there is an associated improvement in clinical outcome. Exploration of how recombinant NRGs alter biomarkers that have been associated with cardiac fibrosis, as well as measurement of fibrosis by non-invasive methods seems warranted in future clinical trials.

Disclosures

Sawyer has received grant support from Acorda Therapeutics, Inc, and has consulted over the development of recombinant NRGs for the treatment of heart failure. Caggiano, Parry, Iaci, and Ganguly are employees and shareholders of Acorda Therapeutics, Inc.

References

1. Falls DL. Neuregulins: functions, forms, and signaling strategies. *Exp Cell Res*. 2003;284:14–30.

2. Liu X, Gu X, Li Z, Li X, Li H, Chang J, Chen P, Jin J, Xi B, Chen D, Lai D, Graham RM, Zhou M. Neuregulin-1/erbB-activation improves cardiac function and survival in models of ischemic, dilated, and viral cardiomyopathy. *J Am Coll Cardiol*. 2006;48:1438–1447.

3. Jabbour A, Hayward CS, Keogh AM, Kotlyar E, McCrohon JA, England JF, Amor R, Liu X, Li XY, Zhou MD, Graham RM, Macdonald PS. Parenteral administration of recombinant human neuregulin-1 to patients with stable chronic heart failure produces favourable acute and chronic haemodynamic responses. *Eur J Heart Fail*. 2011;13:83–92.

4. Gao R, Zhang J, Cheng L, Wu X, Dong W, Yang X, Li T, Liu X, Xu Y, Li X, Zhou M. A Phase II, randomized, double-blind, multicenter, based on standard therapy, placebo-controlled study of the efficacy and safety of recombinant human neuregulin-1 in patients with chronic heart failure. *J Am Coll Cardiol*. 2010;55:1907–1914.

5. Zhao YY, Sawyer DB, Baliga RR, Opel DJ, Han X, Marchionni MA, Kelly RA. Neuregulins promote survival and growth of cardiac myocytes. Persistence of ErbB2 and ErbB4 expression in neonatal and adult ventricular myocytes. *J Biol Chem*. 1998;273:10261–10269.

6. Hill MF, Patel AV, Murphy A, Smith HM, Galindo CL, Pentassuglia L, Peng X, Lenneman CG, Odiete O, Friedman DB, Kronenberg MW, Zheng S, Zhao Z, Song Y, Harrell FE Jr, Srinivas M, Ganguly A, Iaci J, Parry TJ, Caggiano AO, Sawyer DB. Intravenous glial growth factor 2 (GGF2) isoform of neuregulin-1beta improves left ventricular function, gene and protein expression in rats after myocardial infarction. *PLoS One*. 2013;8:e55741.

7. Krombach GA, Kinzel S, Mahnken AH, Gunther RW, Buecker A. Minimally invasive close-chest method for creating reperfused or occlusive myocardial infarction in swine. *Invest Radiol*. 2005;40:14–18.

8. Crick SJ, Sheppard MN, Ho SY, Gebstein L, Anderson RH. Anatomy of the pig heart: comparisons with normal human cardiac structure. *J Anat*. 1998;193:105–119.

9. Livak KJ, Schmittgen TD. Analysis of relative gene expression data using real-time quantitative PCR and the 2(-Delta Delta C(T)) Method. *Methods*. 2001;25:402–408.

10. Ryzhov S, Goldstein AE, Novitskiy SV, Blackburn MR, Biaggioni I, Feoktistov I. Role of A2B adenosine receptors in regulation of paracrine functions of stem cell antigen 1-positive cardiac stromal cells. *J Pharmacol Exp Ther*. 2012;341:764–774.

ORIGINAL RESEARCH

11. Xie Z, Singh M, Siwik DA, Joyner WL, Singh K. Osteopontin inhibits interleukin-1beta-stimulated increases in matrix metalloproteinase activity in adult rat cardiac fibroblasts: role of protein kinase C-zeta. *J Biol Chem*. 2003;278:48546–48552.

12. Ohtani O. Three-dimensional organization of the connective tissue fibers of the human pancreas: a scanning electron microscopic study of NaOH treated-tissues. *Arch Histol Jpn*. 1987;50:557–566.

13. Macchiarelli G, Ohtani O. Endomysium in left ventricle. *Heart*. 2001;86:416.

14. Cote GM, Miller TA, Lebrasseur NK, Kuramochi Y, Sawyer DB. Neuregulin-1alpha and beta isoform expression in cardiac microvascular endothelial cells and function in cardiac myocytes in vitro. *Exp Cell Res*. 2005;311:135–146.

15. Suarez E, Bach D, Cadefau J, Palacin M, Zorzano A, Guma A. A novel role of neuregulin in skeletal muscle. Neuregulin stimulates glucose uptake, glucose transporter translocation, and transporter expression in muscle cells. *J Biol Chem*. 2001;276:18257–18264.

16. Bruer J, Chung KJ, Pesonen E, Haas RH, Guth BD, Sahn DJ, Hesselink JR. Ketone bodies maintain normal cardiac function and myocardial high energy phosphates during insulin-induced hypoglycemia in vivo. *Basic Res Cardiol*. 1989;84:510–523.

17. Breuer J, Chung KJ, Pesonen E, Haas RH, Guth BD, Sahn DJ, Hesselink JR. Cardiac function, substrate utilization, and myocardial energy metabolism studied with 31-P NMR spectroscopy during acute hypoglycemia and hyperketonemia. *Pediatr Res*. 1989;26:536–542.

18. Baliga RR, Pimental DR, Zhao YY, Simmons WW, Marchionni MA, Sawyer DB, Kelly RA. NRG-1-induced cardiomyocyte hypertrophy. Role of PI-3-kinase, p70 (S6K), and MEK-MAPK-RSK. *Am J Physiol Heart Circ Physiol*. 1999;277:H2026–H2037.

19. Grazette LP, Boecker W, Matsui T, Semigran M, Force TL, Hajjar RJ, Rosenzweig A. Inhibition of ErbB2 causes mitochondrial dysfunction in cardiomyocytes: implications for herceptin-induced cardiomyopathy. *J Am Coll Cardiol*. 2004;44:2231–2238.

20. Kuramochi Y, Guo X, Sawyer DB. Neuregulin activates erbB2-dependent src/FAK signaling and cytoskeletal remodeling in isolated adult rat cardiac myocytes. *J Mol Cell Cardiol*. 2006;41:228–235.

21. Guo YF, Zhang XX, Liu Y, Duan HY, Jie BZ, Wu XS. Neuregulin-1 attenuates mitochondrial dysfunction in a rat model of heart failure. *Chin Med J (Engl)*. 2012;125:807–814.

22. Dai F, Lin X, Chang C, Feng XH. Nuclear export of Smad2 and Smad3 by RanBP3 facilitates termination of TGF-beta signaling. *Dev Cell*. 2009;16:345–357.

23. Pan D, Zhe X, Jakkaraju S, Taylor GA, Schuger L. P311 induces a TGF-beta1-independent, nonfibrogenic myofibroblast phenotype. *J Clin Invest*. 2002;110:1349–1358.

24. Lund AK, Goens MB, Nunez BA, Walker MK. Characterizing the role of endothelin-1 in the progression of cardiac hypertrophy in aryl hydrocarbon receptor (AhR) null mice. *Toxicol Appl Pharmacol*. 2006;212:127–135.

25. Fernandez-Salguero P, Pineau T, Hilbert DM, McPhail T, Lee SS, Kimura S, Nebert DW, Rudikoff S, Ward JM, Gonzalez FJ. Immune system impairment and hepatic fibrosis in mice lacking the dioxin-binding Ah receptor. *Science*. 1995;268:722–726.

26. Zaher H, Fernandez-Salguero PM, Letterio J, Sheikh MS, Fornace AJ Jr, Roberts AB, Gonzalez FJ. The involvement of aryl hydrocarbon receptor in the activation of transforming growth factor-beta and apoptosis. *Mol Pharmacol*. 1998;54:313–321.

27. Andreola F, Hayhurst GP, Luo G, Ferguson SS, Gonzalez FJ, Goldstein JA, De Luca LM. Mouse liver CYP2C39 is a novel retinoic acid 4-hydroxylase. Its down-regulation offers a molecular basis for liver retinoid accumulation and fibrosis in aryl hydrocarbon receptor-null mice. *J Biol Chem*. 2004;279:3434–3438.

28. Abbott BD, Schmid JE, Pitt JA, Buckalew AR, Wood CR, Held GA, Diliberto JJ. Adverse reproductive outcomes in the transgenic Ah receptor-deficient mouse. *Toxicol Appl Pharmacol*. 1999;155:62–70.

29. Lehmann GM, Xi X, Kulkarni AA, Olsen KC, Pollock SJ, Baglole CJ, Gupta S, Casey AE, Huxlin KR, Sime PJ, Feldon SE, Phipps RP. The aryl hydrocarbon receptor ligand ITE inhibits TGFbeta1-induced human myofibroblast differentiation. *Am J Pathol*. 2011;178:1556–1567.

30. Tono-Oka S, Tanase S, Miike T, Tanaka H. Transient expression of collagen type XIV during muscle development and its reappearance after denervation and degeneration. *J Histochem Cytochem*. 1996;44:907–918.

31. Tao G, Levay AK, Peacock JD, Huk DJ, Both SN, Purcell NH, Pinto JR, Galantowicz ML, Koch M, Lucchesi PA, Birk DE, Lincoln J. Collagen XIV is important for growth and structural integrity of the myocardium. *J Mol Cell Cardiol*. 2012;53:626–638.

32. Garibaldi BT, D'Alessio FR, Mock JR, Files DC, Chau E, Eto Y, Drummond MB, Aggarwal NR, Sidhaye V, King LS. Regulatory T cells reduce acute lung injury fibroproliferation by decreasing fibrocyte recruitment. *Am J Respir Cell Mol Biol*. 2012;48:35–43.

33. Brzoska E, Kowalewska M, Markowska A, Kowalski K, Archacka K, Zimowska M, Grabowska I, Czerwinska AM, Gora M, Streminska W, Janczyk-Ilach K, Ciemerych MA. The Sdf-1 (CXCL12) improves skeletal muscle regeneration via the mobilization of Cxcr4 and CD34 expressing cells. *Bio Cell*. 2012;104:722–737.

34. Takemoto S, Murakami T, Kusachi S, Iwabu A, Hirohata S, Nakamura K, Sezaki S, Havashi J, Suezawa C, Ninomiya Y, Tsuji T. Increased expression of dermatopontin mRNA in the infarct zone of experimentally induced myocardial infarction in rats: comparison with decorin and type I collagen mRNAs. *Basic Res Cardiol*. 2002;97:461–468.

35. Chereau D, Boczkowska M, Skwarek-Maruszewska A, Fujiwara I, Hayes DB, Rebowski G, Lappalainen P, Pollard TD, Dominguez R. Leiomodin is an actin filament nucleator in muscle cells. *Science*. 2008;320:239–243.

36. Baba H, Ishiwata T, Takashi E, Xu G, Asano G. Expression and localization of lumican in the ischemic and reperfused rat heart. *Jpn Circ J*. 2001;65:445–450.

37. Craig EA, Austin AF, Vaillancourt RR, Barnett JV, Camenisch TD. TGFbeta2-mediated production of hyaluronan is important for the induction of epicardial cell differentiation and invasion. *Exp Cell Res*. 2010;316:3397–3405.

38. Dedieu S, Mazeres G, Poussard S, Brustis JJ, Cottin P. Myoblast migration is prevented by a calpain-dependent accumulation of MARCKS. *Bio Cell*. 2003;95:615–623.

39. Shimazaki M, Nakamura K, Kii I, Kashima T, Amizuka N, Li M, Saito M, Fukuda K, Nishiyama T, Kitajima S, Saga Y, Fukayama M, Sata M, Kudo A. Periostin is essential for cardiac healing after acute myocardial infarction. *J Exp Med*. 2008;205:295–303.

40. Oka T, Xu J, Kaiser RA, Melendez J, Hambleton M, Sargent MA, Lorts A, Brunskill EW, Dorn GW II, Conway SJ, Aronow BJ, Robbins J, Molkentin JD. Genetic manipulation of periostin expression reveals a role in cardiac hypertrophy and ventricular remodeling. *Circ Res*. 2007;101:313–321.

41. Harris BS, Zhang Y, Card L, Rivera LB, Brekken RA, Bradshaw AD. SPARC regulates collagen interaction with cardiac fibroblast cell surfaces. *Am J Physiol Heart Circ Physiol*. 2011;301:H841–H847.

42. McCurdy S, Baicu CF, Heymans S, Bradshaw AD. Cardiac extracellular matrix remodeling: fibrillar collagens and Secreted Protein Acidic and Rich in Cysteine (SPARC). *J Mol Cell Cardiol*. 2010;48:544–549.

43. McCurdy SM, Dai Q, Zhang J, Zamilpa R, Ramirez TA, Dayah T, Nguyen N, Jin YF, Bradshaw AD, Lindsey ML. SPARC mediates early extracellular matrix remodeling following myocardial infarction. *Am J Physiol Heart Circ Physiol*. 2011;301:H497–H505.

44. Bradshaw AD. The role of SPARC in extracellular matrix assembly. *J Cell Commun Signal*. 2009;3:239–246.

45. Bradshaw AD, Baicu CF, Rentz TJ, Van Laer AO, Boggs J, Lacy JM, Zile MR. Pressure overload-induced alterations in fibrillar collagen content and myocardial diastolic function: role of secreted protein acidic and rich in cysteine (SPARC) in post-synthetic procollagen processing. *Circulation*. 2009;119:269–280.

46. Bradshaw AD, Baicu CF, Rentz TJ, Van Laer AO, Bonnema DD, Zile MR. Age-dependent alterations in fibrillar collagen content and myocardial diastolic function: role of SPARC in post-synthetic procollagen processing. *Am J Physiol Heart Circ Physiol*. 2010;298:H614–H622.

47. Atorrasagasti C, Aquino JB, Hofman L, Alaniz L, Malvicini M, Garcia M, Benedetti L, Friedman SL, Podhajcer O, Mazzolini G. SPARC downregulation attenuates the profibrogenic response of hepatic stellate cells induced by TGF-beta1 and PDGF. *Am J Physiol Gastrointest Liver Physiol*. 2011;300:G739–G748.

48. Micheli L, Leonardi L, Conti F, Maresca G, Colazingari S, Mattei E, Lira SA, Farioli-Vecchioli S, Caruso M, Tirone F. PC4/Tis7/IFRD1 stimulates skeletal muscle regeneration and is involved in myoblast differentiation as a regulator of MyoD and NF-kappaB. *J Biol Chem*. 2011;286:5691–5707.

49. Nagai R, Suzuki T, Aizawa K, Shindo T, Manabe I. Significance of the transcription factor KLF5 in cardiovascular remodeling. *J Thromb Haemost*. 2005;3:1569–1576.

50. Young P, Nie J, Wang X, McGlade CJ, Rich MM, Feng G. LNX1 is a perisynaptic Schwann cell specific E3 ubiquitin ligase that interacts with ErbB2. *Mol Cell Neurosci*. 2005;30:238–248.

51. Zhang J, Chang L, Chen C, Zhang M, Luo Y, Hamblin M, Villacorta L, Xiong JW, Chen YE, Zhu X. Rad GTPase inhibits cardiac fibrosis through connective tissue growth factor. *Cardiovasc Res*. 2011;91:90–98.

52. Song K, Nam YJ, Luo X, Qi X, Tan W, Huang GN, Acharya A, Smith CL, Tallquist MD, Neilson EG, Hill JA, Bassel-Duby R, Olson EN. Heart repair by reprogramming non-myocytes with cardiac transcription factors. *Nature*. 2012;485:599–604.

53. Suzuki T, Sawaki D, Aizawa K, Munemasa Y, Matsumura T, Ishida J, Nagai R. Kruppel-like factor 5 shows proliferation-specific roles in vascular remodeling, direct stimulation of cell growth, and inhibition of apoptosis. *J Biol Chem*. 2009;284:9549–9557.

54. Velotta JB, Kimura N, Chang SH, Chung J, Itoh S, Rothbard J, Yang PC, Steinman L, Robbins RC, Fischbein MP. alphaB-crystallin improves murine cardiac function and attenuates apoptosis in human endothelial cells exposed to ischemia-reperfusion. *Ann Thorac Surg*. 2011;91:1907–1913.

55. Eckle T, Hartmann K, Bonney S, Reithel S, Mittelbronn M, Walker LA, Lowes BD, Han J, Borchers CH, Buttrick PM, Kominsky DJ, Colgan SP, Eltzschig HK. Adora2b-elicited Per2 stabilization promotes a HIF-dependent metabolic switch crucial for myocardial adaptation to ischemia. *Nat Med*. 2012;18:774–782.

56. Luther SA, McCullough PA, Havranek EP, Rumsfeld JS, Jones PG, Heidenreich PA, Peterson ED, Rathore SS, Krumholz HM, Weintraub WS, Spertus JA, Masoudi FA. The relationship between B-type natriuretic peptide and health status in patients with heart failure. *J Card Fail*. 2005;11:414–421.

57. Torre-Amione G, Kapadia S, Benedict C, Oral H, Young JB, Mann DL. Proinflammatory cytokine levels in patients with depressed left ventricular ejection fraction: a report from the Studies of Left Ventricular Dysfunction (SOLVD). *J Am Coll Cardiol*. 1996;27:1201–1206.

58. Brittain E, Muldowney JAIII, Geisberg C, Caggiano A, Eisen A, Anderson S, Sawyer D, Mendes L, Lenihan D. Evaluation of cardiac function in symptomatic heart failure patients in a single infusion, phase 1, dose escalation study of glial growh factor 2. *J Am Coll Cardiol*. 2013;61:10_S.